Cell

Antagonistic Control of Social versus Repetitive Self-Grooming Behaviors by Separable Amygdala Neuronal Subsets

Weizhe Hong,[1] Dong-Wook Kim,[2] and David J. Anderson[1,*]
[1]Division of Biology and Biological Engineering, Howard Hughes Medical Institute, California Institute of Technology, Pasadena, CA 91125, USA
[2]Program of Computation and Neural Systems, California Institute of Technology, Pasadena, CA 91125, USA
*Correspondence: wuwei@caltech.edu
http://dx.doi.org/10.1016/j.cell.2014.07.049

SUMMARY

Animals display a range of innate social behaviors that play essential roles in survival and reproduction. While the medial amygdala (MeA) has been implicated in prototypic social behaviors such as aggression, the circuit-level mechanisms controlling such behaviors are not well understood. Using cell-type-specific functional manipulations, we find that distinct neuronal populations in the MeA control different social and asocial behaviors. A GABAergic subpopulation promotes aggression and two other social behaviors, while neighboring glutamatergic neurons promote repetitive self-grooming, an asocial behavior. Moreover, this glutamatergic subpopulation inhibits social interactions independently of its effect to promote self-grooming, while the GABAergic subpopulation inhibits self-grooming, even in a nonsocial context. These data suggest that social versus repetitive asocial behaviors are controlled in an antagonistic manner by inhibitory versus excitatory amygdala subpopulations, respectively. These findings provide a framework for understanding circuit-level mechanisms underlying opponency between innate behaviors, with implications for their perturbation in psychiatric disorders.

INTRODUCTION

Animals exhibit a broad range of innate behaviors that are essential for their survival and reproduction. These include responses to predators or prey, social behaviors among conspecifics, as well as solitary behaviors such as self-grooming (Tinbergen, 1951). The control of innate social behaviors, while observed throughout the animal kingdom, is of particular importance in social species such as humans (Stanley and Adolphs, 2013). Abnormalities in social behaviors are associated with several psychiatric disorders (Couture et al., 2010; Sasson et al., 2007).

An important brain region implicated in the control of innate social behaviors is the medial amygdala (MeA) (Kondo, 1992; Kondo and Arai, 1995; Lehman et al., 1980; Newman, 1999). The MeA is one of over a dozen subdivisions of the amygdala (Pitkänen et al., 1997; Swanson and Petrovich, 1998) and is anatomically distinct from amygdala nuclei involved in conditioned fear (Duvarci and Pare, 2014; Ehrlich et al., 2009; Paré et al., 2004). It is located only two synapses away from the vomeronasal organ (VNO), a sensory epithelium that detects pheromonal signals (Dulac and Torello, 2003; Zufall and Leinders-Zufall, 2007), and projects to hypothalamic regions involved in social and other motivated behaviors (Swanson, 2000). Thus, the MeA is situated at an early stage in sensory information processing, suggesting that it may function at a relatively high level in behavioral decision hierarchies (Tinbergen, 1951).

MeA neurons are active during social behaviors such as fighting and mating and in response to chemosensory cues, as evidenced by induction of c-*fos*, a surrogate marker of neuronal activity (Choi et al., 2005; Erskine, 1993; Kollack and Newman, 1992; Kollack-Walker and Newman, 1995; Veening et al., 2005), as well as by electrophysiology (Bergan et al., 2014; Bian et al., 2008). Although lesion studies have implicated the MeA in male mating (Kondo, 1992; Kondo and Arai, 1995; Lehman et al., 1980), in the case of aggression the direction of its influence is not clear: in some studies MeA lesions decreased aggression (Kemble et al., 1984; Takahashi and Gladstone, 1988; Wang et al., 2013), while in others they increased it or had no effect (Busch and Barfield, 1974; Rosvold et al., 1954; Vochteloo and Koolhaas, 1987).

The conclusion that the MeA plays a role in social behavior leaves open the question of how it performs this function. On the one hand, the MeA may control social behaviors in a positive-acting manner. In the simplest version of this hypothesis, activation of MeA neurons in response to chemosensory cues would promote social behavior, while in the absence of such activity social behavior would not occur (Figure S1A available online). However, the MeA is known to contain heterogeneous neuronal subpopulations (Bian et al., 2008; Choi et al., 2005; Niimi et al., 2012; Xu et al., 2012), whose functions in social behavior are unknown. This raises the possibility that the MeA may control social behaviors in a more complex manner that involves distinct cell types, which may have different or even opponent roles (Figure S1B).

Here, we have investigated the cellular control of social behavior by performing functional manipulations of distinct

neuronal subpopulations within the posterior dorsal subdivision of MeA (MeApd) (Canteras et al., 1995; Dong et al., 2001; Swanson, 2000). Our experiments reveal that GABAergic neurons in MeApd promote aggression as well as two other innate social behaviors, mating and social grooming. In contrast, neighboring but nonoverlapping glutamatergic neurons in MeApd (and adjacent LHA) promote repetitive self-grooming, an asocial behavior. Moreover, the glutamatergic neurons inhibit social behaviors, in a manner independent of their effect to promote self-grooming. Conversely, GABAergic MeApd neurons suppress self-grooming, in both social and nonsocial contexts. Thus, the MeApd controls both social and repetitive asocial behaviors, via nonoverlapping subpopulations of inhibitory and excitatory neurons, respectively, each of which exerts both positive-acting and antagonistic, negative-acting influences.

RESULTS

Functional Identification of MeApd in Aggressive Behavior

The MeApd has been implicated in social behaviors (Newman, 1999; Swanson, 2000). As a first step toward dissecting the function of MeApd, we focused on offensive intermale aggression between conspecifics, a prototypic social behavior (Adams, 2006; Blanchard et al., 2003; Kruk, 1991; Siegel et al., 1999). c-*fos* induction studies have shown that the MeApd is activated during offensive aggression (Lin et al., 2011; Nelson and Trainor, 2007; Newman, 1999; Veening et al., 2005). We confirmed that MeApd exhibits elevated expression of c-*fos* in resident males that had recently attacked an intruder (Figures 1A–1D). To determine whether c-*fos* expression is associated with attack, or simply with exposure to conspecific sensory cues, we compared its induction during aggression versus social investigations that did not lead to attack (Figures 1B and 1C). Social investigation in the latter cases occupied ~40% of the total observation period and was associated with an ~3-fold increase in c-*fos* expression. However, the level of c-*fos* expression in MeApd following episodes of attack was much higher (Figures 1B–1D). Thus, MeApd is active during both social investigation and attack, but more strongly so during the latter, similar to our recent observations in the ventrolateral subdivision of the ventromedial hypothalamus (VMHvl) (Lee et al., 2014).

Although lesion studies have suggested that MeApd is involved in aggression, the evidence regarding the valence of its influence is contradictory. Therefore, it was not clear whether activation of MeApd neurons would promote or inhibit attack. Moreover, while MeApd is activated by pheromonal signals (Chamero et al., 2007; Kollack-Walker and Newman, 1995; Veening et al., 2005), attack requires chemosensory input from the main as well as the accessory olfactory systems (Dhungel et al., 2011; Mandiyan et al., 2005; Stowers et al., 2002; Yoon et al., 2005). This raises the question of where in this circuitry such convergent sensory input is transformed into a coherent program of aggressive behavior. On the one hand, this transformation might occur in structures downstream of MeApd, such as VMHvl (Lee et al., 2014; Lin et al., 2011; Yang et al., 2013); on the other hand, MeApd itself might be sufficient to evoke attack.

To distinguish between these alternatives, we injected wild-type C57BL/6N male mice with a mixture of AAV viruses encoding Cre (CMV-Cre) and a Cre-dependent channelrhodopsin 2 (ChR2) (Boyden et al., 2005) (Figures 1E and S2A). The ChR2 virus (AAV-EF1α-FLEX-ChR2-2A-hrGFP) contained a nuclear hrGFP reporter (Lee et al., 2014), allowing visualization of ChR2-expressing cell bodies (Figures 1E, 1F and S2A). Successful photostimulation of MeApd neurons in vivo via an implanted optic fiber (Aravanis et al., 2007) was confirmed by double labeling for hrGFP and c-*fos* (Figures 1F–1G).

We examined next the behavioral effects of optogenetic stimulation of MeApd neurons in resident mice in their home cage under infrared light, using the resident-intruder assay (Blanchard et al., 2003). We focused our studies on offensive aggression, a form of aggression that consists of biting and tussling and is initiated by resident animals (see Experimental Procedures). To avoid any intruder-initiated aggression, a more submissive mouse was used as the intruder (see Experimental Procedures). The sessions were video recorded in a customized chamber with two synchronized infrared video cameras at a 90° angle (Figures 1H and S3).

Optogenetic activation of MeApd elicited intense, time-locked attack toward intruder males, castrated males, and females (Figures 1I and 1J; Movie S1). To reliably measure the level of time-locked activation of attack that is induced by optogenetic stimulation, we minimized the baseline aggression level by group housing resident animals prior to the virus injection and fiber implantation (see Experimental Procedures). In these ChR2-expressing males, attack was triggered toward male intruders in 100% of ChR2-expressing animals and over 60% of the trials; attack was also triggered toward castrated males and female intruders (Figures 1K and 1L). Attack evoked by optogenetic stimulation included both biting and tussling (Movie S1), similar to the pattern of naturally occurring attack behavior in unmanipulated animals (Kruk, 1991; Kruk et al., 1998; Siegel et al., 1999). Furthermore, attack was initiated at the onset and ceased after the offset of photostimulation, with short latencies (Figures 1M and 1N). Episodes of attack occupied 45%–60% of the photostimulation period (Figure 1O). Animals expressing a control EYFP virus in MeApd failed to show any photostimulation-evoked aggression (Figures 1I, 1K, 1L, and 1O). These data indicate that activation of MeApd neurons using a generic promoter can promote aggression.

GABAergic Neurons in MeApd Promote Aggressive Behavior

To determine whether attack can be triggered by optogenetic stimulation of a specific, genetically defined population within MeApd, we sought to identify lines of Cre recombinase-expressing mice that could be used to manipulate distinct subsets of MeApd neurons. MeApd consists of both vGAT$^+$ (GABAergic) and vGLUT2$^+$ (glutamatergic) neurons (Choi et al., 2005), but they are differentially distributed along the medio-lateral axis: vGAT$^+$ neurons are distributed throughout MeApd whereas vGLUT2$^+$ neurons are preferentially enriched in the medial region (Bian et al., 2008) (Figures 2A–2D). We therefore investigated whether GABAergic and/or glutamatergic neurons might contain aggression-promoting cells.

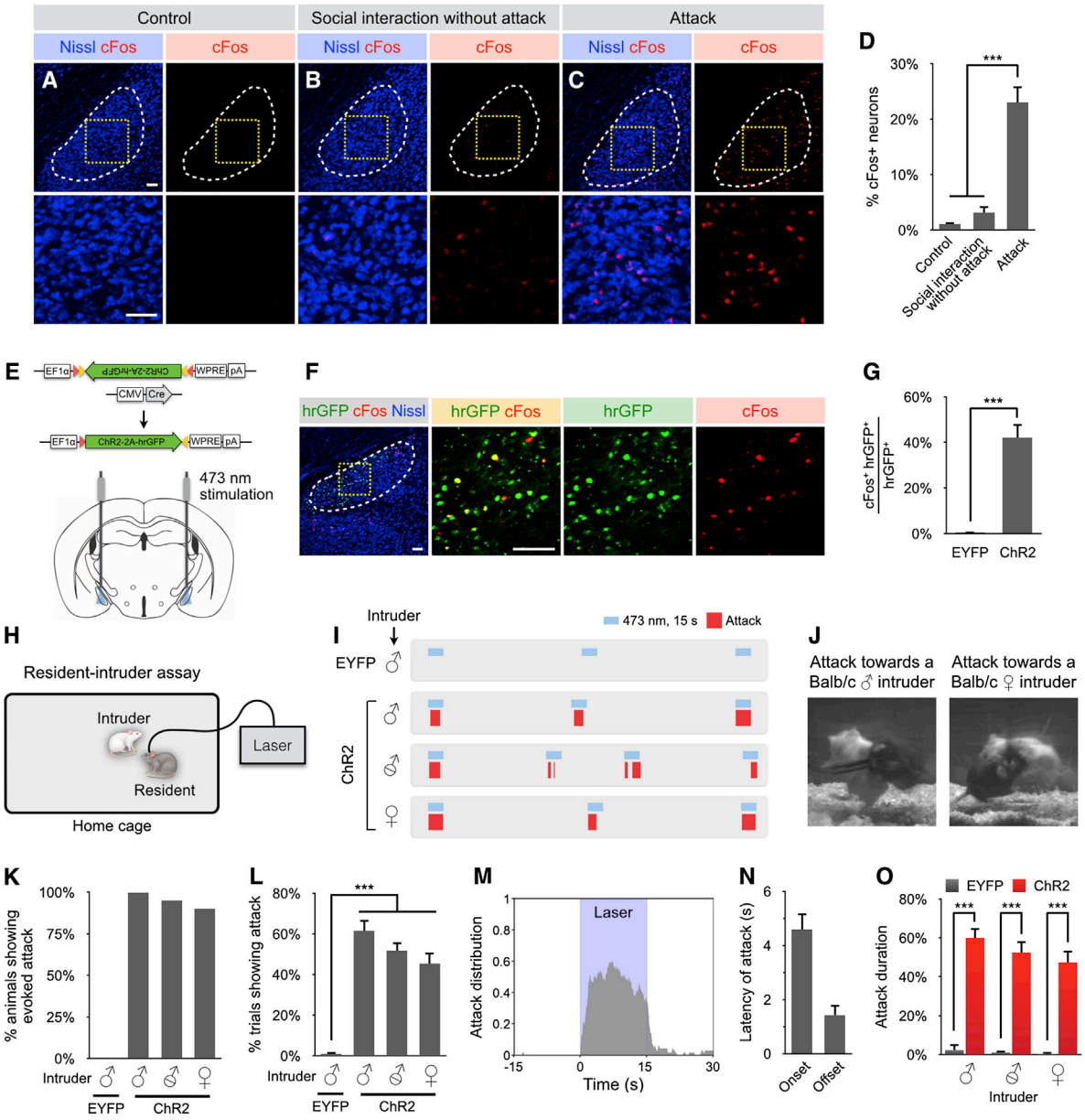

Figure 1. Functional Identification of MeApd in Aggressive Behavior

(A–D) c-*fos* induction in C57BL/6N resident males following offensive attack, or social interaction without attack, toward intruder males. Red, c-*fos* immunostaining; blue, fluorescent Nissl stain. Scale bars represent 100 μm. (D) Percentage of cells expressing c-*fos* in each condition. n = 5 animals for each condition.

(E) Schematic illustrating ChR2 virus injection and optic fiber placement site.

(F and G) c-*fos* induction in EF1α::ChR2-hrGFP-expressing MeApd neurons in a solitary animal at 1 hr postillumination. Red, c-*fos* immunostaining; green, hrGFP native fluorescence; blue, fluorescent Nissl stain. Scale bars represent 50 μm. (G) Percentage of total $hrGFP^+$ cells that express c-*fos*. n = 4 animals for each condition.

(H) Schematic illustrating the resident-intruder assay. See Experimental Procedures and Figure S3.

(I–O) Optogenetic stimulation of MeApd triggers attack. (I) Representative raster plots illustrating attack episodes in control EYFP or ChR2-expressing males tested with BALB/c intruders (male, castrated male, female) in the resident-intruder assay. (J) Video frames taken from attack episodes. (K) Percentage of resident males that display attack. (L) Percentage of trials showing light-induced attack using laser power 1–3 mW mm^{-2}. (M) Distribution of attack episodes (percentage of trials showing attack at different time points) with respect to the initiation of laser illumination. (N) Attack onset and offset latencies (relative to initiation and termination of illumination, respectively). (O) Percentage of time spent attacking during photostimulation period. (K and L) n ≥ 10 animals for each condition. (M and N) n = 118 trials. (O) n ≥ 30 trials for each condition.

Data are mean ± SEM. ***p < 0.001. See also Figures S1, S2, and S3 and Movie S1.

We first asked whether GABAergic and/or glutamatergic neurons are activated during attack, using c-*fos* induction. Existing antibodies to GABAergic markers do not provide cellular resolution in the MeA (data not shown), precluding a quantitative comparison with c-*fos* expression. Therefore, we generated double heterozygous male mice that expressed both vGAT-Cre (Vong et al., 2011) and a Cre-dependent reporter ZsGreen (Ai6) (Madisen et al., 2010), which provides strong cell body labeling. Double labeling for c-*fos* and ZsGreen in males that had recently attacked an intruder (Figures 2A–2D) revealed, surprisingly, that more than 90% of the c-*fos*$^+$ neurons were ZsGreen$^+$, suggesting the majority of c-*fos*$^+$ neurons induced by attack are vGAT$^+$ (Figures 2A, 2B, and 2E). In contrast, in double-transgenic animals that expressed vGLUT2-Cre and ZsGreen, <10% of the c-*fos*$^+$ neurons were ZsGreen$^+$ following attack (Figures 2C–2E). Furthermore, ~30% of the vGAT$^+$ neurons were c-*fos*$^+$, whereas ~3% of the vGLUT2$^+$ neurons were c-*fos*$^+$ (Figure S2E). In control animals that did not experience social interactions, little overlap was observed between c-*fos*$^+$ and ZsGreen$^+$ neurons (data not shown). These data suggest that neurons in MeApd that are activated during attack behavior are predominantly vGAT$^+$.

To determine whether attack could be triggered by optogenetic activation of GABAergic neurons in MeApd, we injected vGAT$^{Cre/+}$ male mice with a rAAV virus encoding a Cre-dependent ChR2 (Figures 2F and S2B). Whole-cell patch clamp recordings in acute MeA brain slices confirmed that photostimulation elicited action potentials from ChR2-expressing vGAT$^+$ cells with high fidelity (Figures 2G–2I). Successful photostimulation of ChR2-expressing vGAT$^+$ neurons in vivo via an implanted optic fiber was confirmed by double labeling for hrGFP and c-*fos* (Figures 2J–2L).

Optogenetic stimulation of vGAT$^+$ neurons in MeApd triggered intense attack in all ChR2-expressing animals (Figures 2M and 2N; Movie S2). Attack was triggered toward male intruders in over 90% of the trials and toward castrated males and female intruders in 75%–80% of the trials (Figure 2O), with short latency relative to the onset of photostimulation (Figures 2P and 2Q). When light pulses were delivered under optimal conditions (the resident facing the intruder and within half a body-length) (Lee et al., 2014; Lin et al., 2011), attack was triggered within ~1 s of photostimulation (Figure 2Q). Attack, on average, lasted 60%–85% of the stimulation period (Figure 2R). Photostimulation of MeApd GABAergic neurons also evoked attack toward a toy mouse (Figure 2S), suggesting that olfactory cues are not essential for optogenetically evoked aggression and also that attack is not due to a defect in sex discrimination (Lee et al., 2014; Lin et al., 2011).

GABAergic Neuron Activity in MeApd Is Required for Ongoing Aggressive Behavior

We next addressed the requirement of MeApd vGAT$^+$ neuronal activity for aggression in a time-resolved manner, via optogenetic inhibition using a Cre-dependent rAAV encoding eNpHR3, a light-driven chloride pump (Gradinaru et al., 2010), in vGAT$^{Cre/+}$ male mice (Figures 3A and S2D). Efficient photostimulation-dependent (593 nm) silencing of vGAT$^+$ neurons was confirmed by whole-cell patch clamp recording in acute MeApd brain slices prepared from virally injected animals (Figures 3B and 3C).

We examined the behavioral effects of optogenetically silencing MeApd vGAT$^+$ neurons (Figures 3D and 3E). To reliably examine time-resolved suppression of attack, we preselected resident animals with higher levels of baseline attack based on pilot resident-intruder trials without photostimulation (see Experimental Procedures). Photostimulation of a resident mouse in its home cage was applied for 3 s, after the onset of spontaneous aggressive encounters with a male intruder. In response to optogenetic inhibition, males stopped attacking in <1 s in 97% of the photostimulation trials, with an average latency <0.5 s (Figures 3E–3J; Movie S3). Similarly, optogenetic silencing of MeApd neurons in wild-type mice using a generic EF1α promoter-driven eNpHR3 also interrupted attack (Figures 3F, 3I, 3J, and S4). In contrast, control males expressing EYFP continued to attack the intruder in over 90% of stimulation trials (Figures 3E–3G, 3I, and 3J). These data indicated that ongoing activity in MeApd vGAT$^+$ neurons is required for naturally occurring attack behavior.

GABAergic Neurons Control Different Social Behaviors at Different Stimulation Intensities

The foregoing data indicated that vGAT$^+$ neurons in MeApd are both necessary and sufficient for aggressive behavior. We next asked whether MeApd vGAT$^+$ neurons could also promote other social behaviors. Our previous studies showed that photostimulation of VMHvl neurons at different light intensities triggered different social behaviors: low intensity photostimulation triggered sniffing and mounting behavior, while high intensity photostimulation triggered attack (Lee et al., 2014). To determine whether this phenomenon is also characteristic of MeApd, we performed optogenetic stimulation of vGAT$^+$ neurons across a wide range of illumination intensities (Figure 4A). Indeed, low intensity stimulation triggered mounting behavior toward intact and castrated males, as well as female intruders (Figures 4A and 4B; Movie S4). As the intensity of stimulation was increased, evoked behaviors in the same animals switched from mounting to attack (Figures 4C and 4D). At intermediate light intensities, photostimulation triggered a mixture of attack and mounting behavior (Figure 4A).

Interestingly, low intensity stimulation of MeApd vGAT$^+$ neurons also triggered social grooming behavior toward intact and castrated males (Figures 4B and 4E), a behavior not observed in the VMHvl-stimulated animals (Lee et al., 2014). As the light intensity was increased, we observed a transition from social grooming to attack in the same mice (Figures 4F and 4G). Interestingly, low intensity stimulation triggered social grooming in some animals and mounting in other animals. Attempts to separate these behaviors by systematically manipulating stereotaxic injection coordinates within MeApd were unsuccessful (data not shown). Together, these data indicate that optogenetic activation of vGAT$^+$ neurons in MeApd, as in VMHvl (Lee et al., 2014), can promote multiple social behaviors in an intensity-dependent manner.

Neighboring Glutamatergic Neurons Promote Self-Grooming Behavior

The foregoing data indicated that vGAT$^+$ neurons in MeApd can promote multiple social behaviors. This observation raised the question of whether other subpopulations of MeApd neurons would also promote such social behaviors. Since MeApd

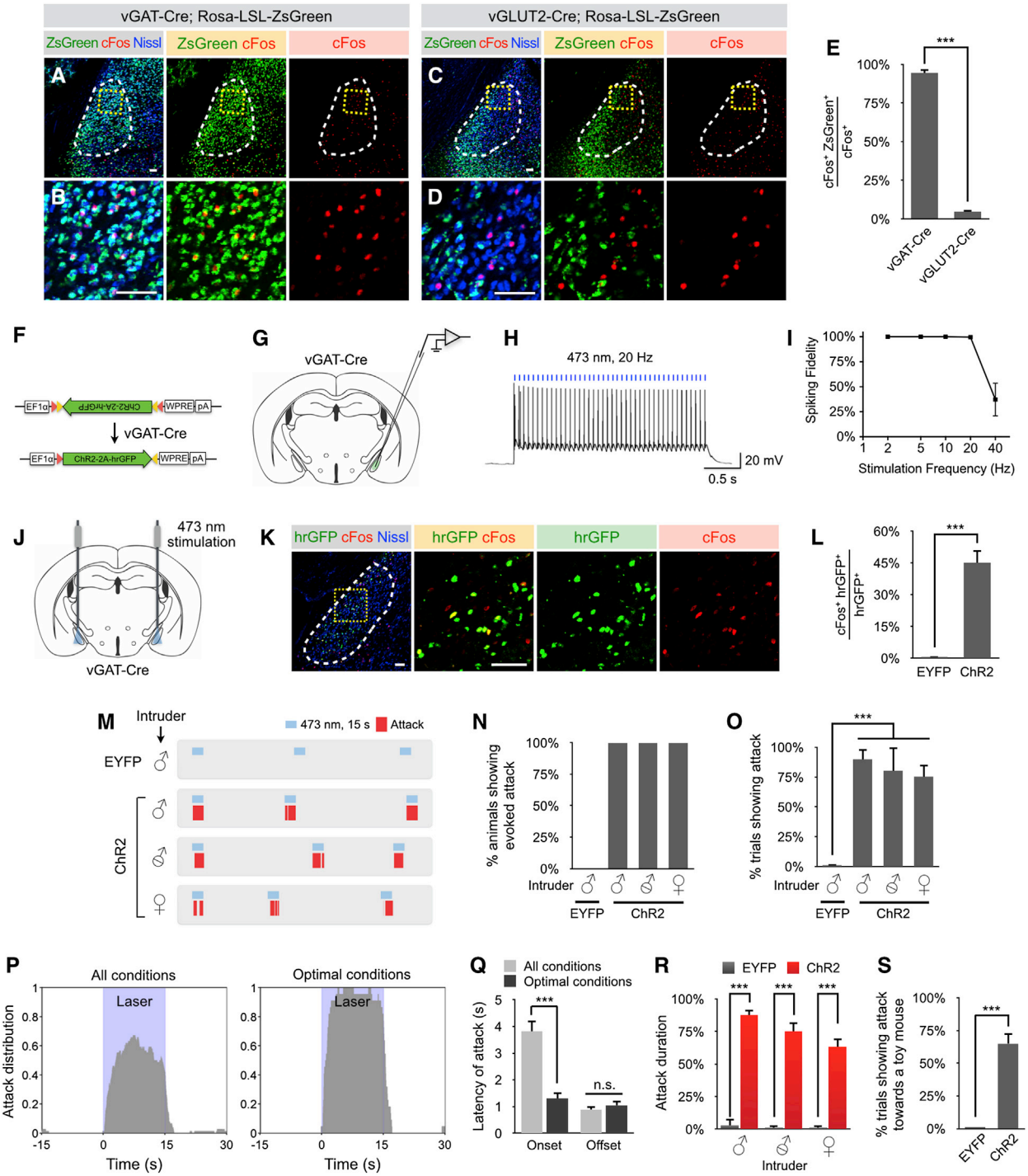

Figure 2. Optogenetic Stimulation of vGAT$^+$ Neurons in MeApd Triggers Aggressive Behavior

(A–E) vGAT$^+$ neurons in MeApd are activated during aggressive behavior. (A–D) c-*fos* induction in vGAT$^{Cre/+}$ or vGLUT2$^{Cre/+}$ resident males following attack toward intruder males. Resident males are double heterozygous for vGAT-Cre and Rosa-LSL-ZsGreen (Ai6), or double heterozygous for vGLUT2-Cre and Rosa-LSL-ZsGreen (Ai6). Red, c-*fos* immunostaining; green, ZsGreen native fluorescence; blue, fluorescent Nissl stain. Scale bars represent 50 μm. (E) Percentage of ZsGreen$^+$ cells expressing c-*fos*. n = 4 animals for each condition.

(F) Schematic illustrating the ChR2 virus injected.

(G–I) Whole-cell patch clamp recording from vGAT$^+$ cells in MeApd in acute brain slices. (H) Photostimulation-evoked spiking (473 nm) and (I) quantification of spike fidelity are shown (n = 5 cells).

(J) Schematic illustrating the optic fiber placement in vGAT$^{Cre/+}$ animals.

(legend continued on next page)

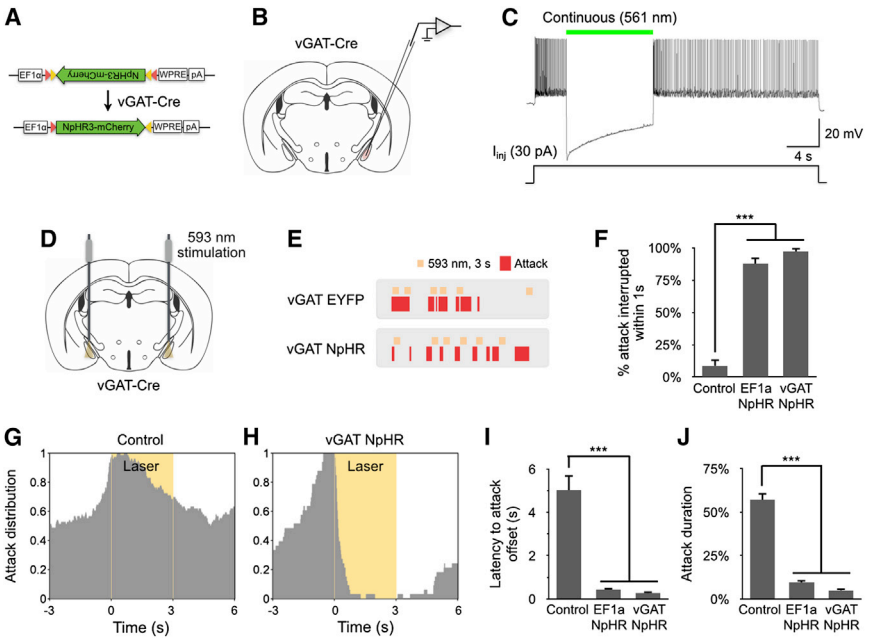

Figure 3. The Activity of MeApd vGAT$^+$ Neurons Is Required for Ongoing Aggressive Behavior

(A) Schematic illustrating the Cre-dependent eNpHR3 virus injected in vGAT$^{Cre/+}$ animals.

(B and C) Whole-cell patch clamp recording in acute brain slices, showing photostimulation-induced suppression of current injection-evoked spiking in eNpHR3-mCherry expressing vGAT$^+$ cells in MeApd (C).

(D) Schematic illustrating the optic fiber placement in vGAT$^{Cre/+}$ animals.

(E) Representative raster plots illustrating attack episodes in control or eNpHR3-expressing males tested with intact BALB/c male intruders in the resident-intruder assay.

(F) Percentage of attack episodes interrupted within 1 s after the initiation of the laser illumination.

(G and H) Distribution of attack episodes (percentage of trials showing attack at different time points) with respect to the initiation of laser illumination in control or eNpHR3-expressing males paired with male intruders.

(I) Latencies to interrupt attack with respect to the initiation of the laser illumination.

(J) Percentage of time spent attacking during the 3 s photostimulation period

Data are mean ± SEM. ***$p < 0.001$. In (F)–(J), n = 116 trials for control, n = 81 trials for EF1α eNpHR3, and n = 63 trials for vGAT eNpHR3. See also Figures S2 and S4 and Movie S3.

contains both glutamatergic and GABAergic neurons (Figures 2A–2D), we next targeted the glutamatergic population marked by expression of vGLUT2.

We injected vGLUT2$^{Cre/+}$ male mice (Vong et al., 2011) with an rAAV virus encoding a Cre-dependent ChR2 (Figures 5A and S2C). Whole-cell patch clamp recordings in acute MeApd brain slices confirmed that photostimulation elicited action potentials from ChR2-expressing vGLUT2$^+$ cells with high temporal precision and high spike fidelity (Figures 5B–5D). Successful photostimulation of vGLUT2$^+$ neurons in vivo via an implanted optic fiber was confirmed by double labeling for hrGFP and c-*fos* (Figures 5E–5G).

We then examined behaviorally the effect of optogenetic stimulation of vGLUT2$^+$ neurons in resident mice exposed to an intruder. Interestingly, photostimulation did not elicit any attack, mounting, or social grooming behavior in the presence of an intruder of any sex (Figures 5H–5J). Instead, photostimulation elicited robust, repetitive self-grooming behavior with short latency in all ChR2-expressing vGLUT2$^{Cre/+}$ animals tested (Figures 5H–5L and 5N). Self-grooming behavior was also observed when stimulation was applied to solitary animals (Figures 5H, 5M, and 5N). The self-grooming behavior evoked by optogenetic stimulation consisted of paw licking, facial grooming as well as body grooming (Movie S5), similar to the pattern of spontaneous self-grooming behavior in wild-type animals. Importantly, optogenetic stimulation of vGLUT2$^+$ neurons did not evoke any other nonsocial behaviors, such as locomotion, freezing, jumping, feeding or drinking. Finally, self-grooming behavior was not triggered by inhibition of naturally occurring attack via optogenetic silencing of vGAT$^+$ neurons (Figure S6E), or during the offset of optogenetically activated aggression, arguing that this repetitive behavior is not simply a default activity that invariably occurs when an ongoing social behavior such as aggression is interrupted.

Interestingly, the self-grooming behavior triggered by the activation of vGLUT2$^+$ neurons persisted for several seconds after the termination of the stimulation (Figures 5L and 5O). The persistent effect was greater in solitary animals when no intruder was present (Figures 5M and 5O). Whether this persistence reflects a persistent internal brain state, or is

(K and L) c-*fos* induction in EF1α::ChR2-hrGFP-expressing vGAT$^+$ neurons in solitary animals at 1 hr postillumination. Red, c-*fos* immunostaining; green, hrGFP native fluorescence; blue, fluorescent Nissl stain. Scale bars represent 50 μm. (L) Percentage of hrGFP$^+$ cells expressing c-*fos*. n = 4 animals for each condition. (M–S) Optogenetic stimulation of MeApd vGAT$^+$ neurons triggers attack. (M) Representative raster plots illustrating attack episodes in control or ChR2-expressing vGAT$^{Cre/+}$ males tested with BALB/c intruders (male, castrated male, female) in the resident-intruder assay. (N) Percentage of resident males that displayed attack. (O) Percentage of trials showing light-induced attack using laser power 1–3 mW mm^{-2}. (P) Distribution of attack episodes (percentage of trials showing attack at different time points) with respect to the initiation of laser illumination. Left panel, all conditions; right panel, optimal conditions (resident was facing the intruder and within half a body-length). (Q) Attack onset and offset latencies (relative to initiation and termination of illumination, respectively). (R) Percentage of time spent attacking during photostimulation period. (S) Percentage of trials showing optogenetically evoked attack toward an inanimate toy mouse. (N and O) n ≥ 10 animals for each condition. (P and Q) n = 93 trials for all conditions and n = 22 trials for optimal conditions. (R) n ≥ 25 trials for each condition. (S) n = 5 animals for each condition.

Data are mean ± SEM. n.s., $p > 0.05$, ***$p < 0.001$. See also Figures S2 and S5 and Movie S2.

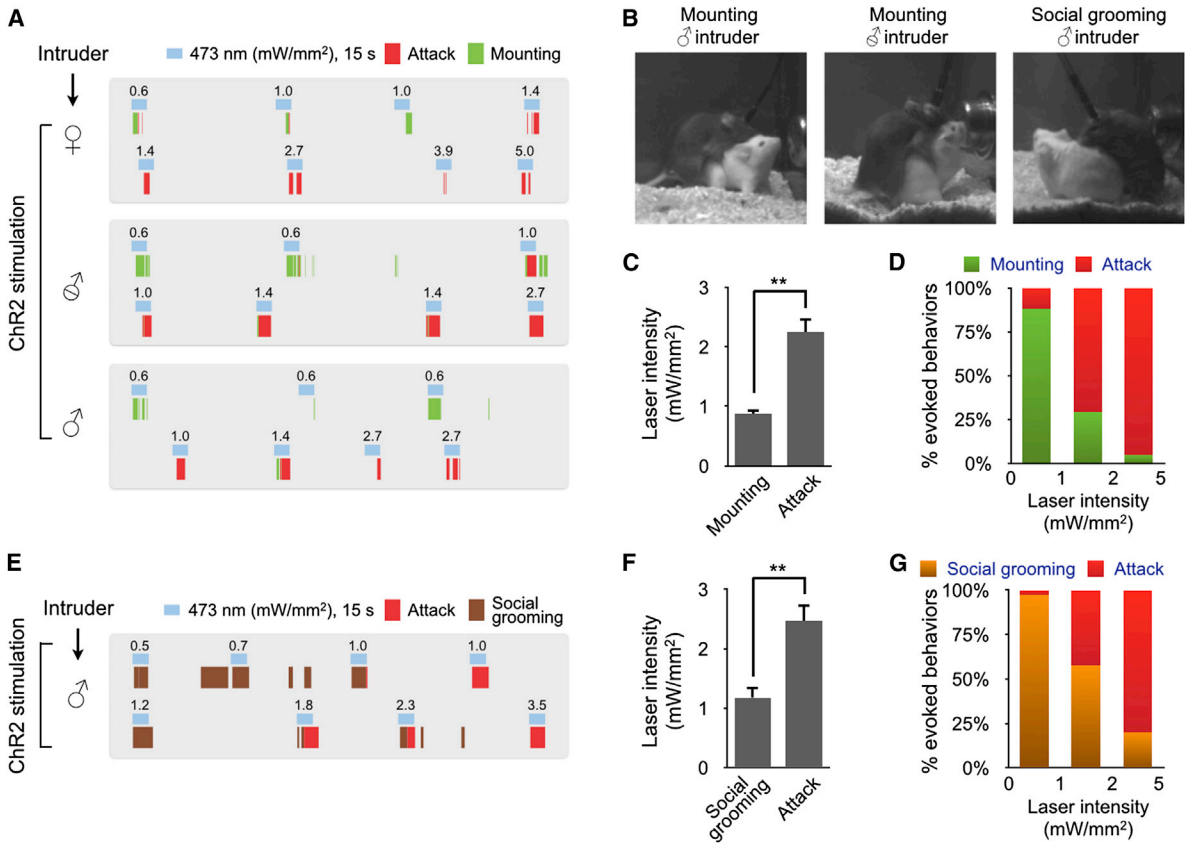

Figure 4. MeApd vGAT⁺ Neurons Control Different Social Behaviors in a Scalable Manner

(A and E) Representative raster plots illustrating different social behavior episodes in control or ChR2-expressing males tested with BALB/c intruders (male, castrated male, female) in the resident-intruder assay. Laser pulses were delivered at different indicated illumination intensities.

(B) Video frames taken from behavioral episodes with BALB/c male (intact or castrated) intruders.

(C and F) Average laser illumination intensities that trigger different social behaviors. n ≥ 40 trials for each condition.

(D and G) Percentage of evoked behaviors at different ranges of laser illumination intensities. Upon low intensity stimulation, we observed mounting in 8 animals and social grooming in six animals. n ≥ 40 trials for each condition.

Data are mean ± SEM. **p < 0.01. See also Movie S4.

promoted by positively reinforcing sensory feedback, is not yet clear.

The effect of optogenetic activation to trigger self-grooming was also highly specific to vGLUT2⁺ neurons, as stimulation of vGAT⁺ neurons did not trigger any self-grooming behavior (Figures 5I and 5J). Interestingly, when MeApd neurons were photostimulated with ChR2 expressed nonselectively in wild-type animals (see Figure 1E), a mixture of both attack and repetitive self-grooming was observed (Figures 5I and 5J). The elicitation of both behaviors at a single injection site using a ubiquitous promoter likely reflects a coactivation of both GABAergic and glutamatergic neurons, emphasizing the functional heterogeneity of MeApd.

When ChR2 virus was injected into MeApd, its expression occasionally spread into the adjacent lateral hypothalamic area (LHA), a small region medial to MeApd (Figure S5). To determine whether there is any spatial specificity within MeApd and adjacent LHA in triggering different behaviors, ChR2 virus was injected into different locations in MeApd and adjacent LHA using modified stereotaxic coordinates (see Experimental Procedures). The anatomical distribution of ChR2-expressing neurons in these injected animals is illustrated in Figure S5D. These studies indicated that the vGAT⁺ neurons that trigger attack are located within the MeApd (Figure S5E). Self-grooming could be triggered when the majority of ChR2-expressing vGLUT2⁺ neurons are located in MeApd (Figure S5F). It could also be triggered, to a lesser extent, by injections into the lateral part of LHA (Figure S5F). Thus, the excitatory neurons that promote self-grooming are interspersed and/or juxtaposed with the inhibitory neurons that promote social behaviors.

Glutamatergic Neurons Suppress Social Behaviors

Because activation of glutamatergic neurons promoted repetitive self-grooming, we next examined whether optogenetic stimulation of vGLUT2⁺ neurons during an ongoing social behavior would interrupt the latter in a dominant manner. Indeed, stimulation of ChR2-expressing vGLUT2⁺ MeApd neurons interrupted naturally occurring attack in <3 s, in over 75% of the stimulation

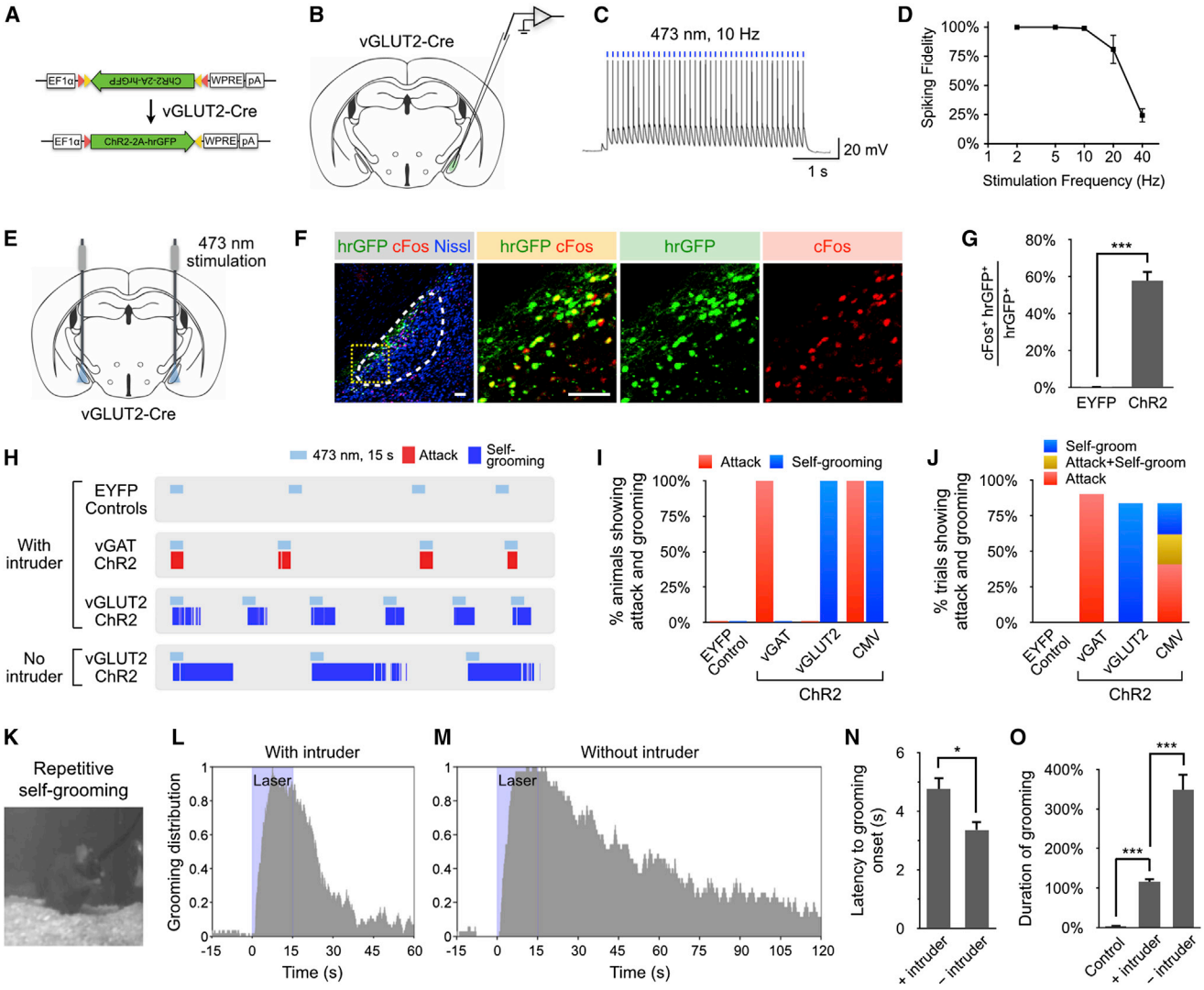

Figure 5. Neighboring vGLUT2$^+$ Neurons Promote Self Grooming

(A) Schematic illustrating the ChR2 virus injected.

(B–D) Whole-cell patch clamp recording from vGLUT2$^+$ cells in MeApd in acute brain slices. Photostimulation-evoked spiking (473 nm) (C) and quantification of spike fidelity (D) are shown. (D) n = 4 cells.

(E) Schematic illustrating optic fiber placement in vGLUT2$^{Cre/+}$ animals.

(F and G) c-*fos* induction in EF1α::ChR2-hrGFP-expressing vGLUT2$^+$ neurons in solitary animals at 1 hr postillumination. Red, c-*fos* immunostaining; green, hrGFP native fluorescence; blue, fluorescent Nissl stain. Scale bars represent 50 μm. (G) Percentage of total hrGFP$^+$ cells expressing c-*fos*. n = 4 animals for each condition.

(H) Representative raster plots illustrating self-grooming episodes in EYFP control and ChR2-expressing males in the presence or absence of intact BALB/c intruder males.

(I) Percentage of resident males showing evoked attack or self-grooming. CMV: Nonselective expression of ChR2 in MeApd by coinjecting AAVs expressing CMV-Cre and Cre-dependent ChR2. n ≥ 10 animals for each condition.

(J) Percentage of trials showing evoked attack or self-grooming using laser power 1–3 mW mm^{-2}. n ≥ 10 animals for each condition.

(K) Video frame taken from repetitive self-grooming episodes.

(L and M) Distribution of self-grooming episodes (percentage of trials showing self-grooming at different time points) with respect to the initiation of laser illumination in ChR2-expressing males in the presence or absence of intruder animals. Data are normalized on a scale of 0–1.

(N) Onset latencies of self-grooming relative to the initiation of illumination.

(O) Percentage of time spent self-grooming during the 15 s photostimulation period. (L–O) n = 79 trials for ChR2 animals with intruders, n = 37 trials for ChR2 animals without intruders, and n = 25 trials for control.

Data are mean ± SEM. *p < 0.05, ***p < 0.001. See also Figures S2 and S5 and Movie S5.

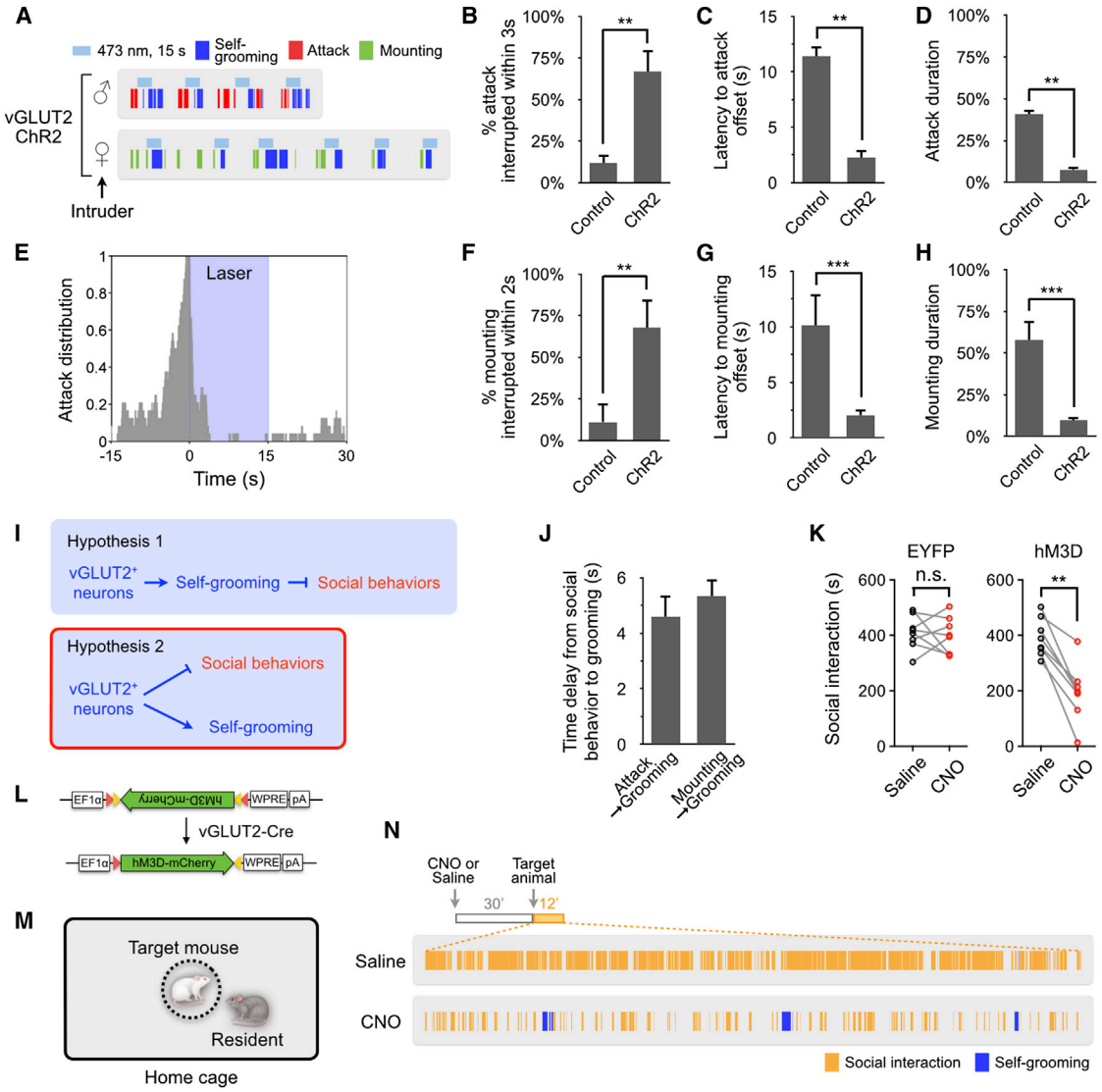

Figure 6. vGLUT2⁺ Neurons Suppress Naturally Occurring Social Behaviors

(A–H and J) ChR2 activation of vGLUT2⁺ neurons suppresses ongoing social behavior. (A) Representative raster plots illustrating attack, mounting, and self-grooming behavior in the presence of BALB/c intruder mice. (E) Distribution of attack episodes (percentage of trials showing attack at different time points) with respect to the initiation of laser illumination in ChR2-expressing males. (B and F) Percentage of attack or mounting episodes interrupted within seconds after the initiation of the laser illumination. (C and G) Latency to stop attack or mounting with respect to the initiation of the laser illumination. (D and H) Percentage of attack or mounting during the 15 s photostimulation period. (J) Time delay when transitioning from the interruption of ongoing social behavior to the onset of self-grooming. (A–E) n ≥ 24 trials for each condition. (F–H and J) n ≥ 17 trials for each condition.

(I) Two alternative hypotheses of how vGLUT2⁺ neurons suppress social behaviors.

(K–N) Pharmacogenetic activation of vGLUT2⁺ neurons reduces social interaction in a modified resident intruder assay. (L) Schematic illustrating the Cre-dependent hM3D virus injected. (M) Illustration of modified resident intruder assay (intruder target mice are confined in an inverted pencil cup). (N) Representative raster plots illustrating social interaction and self-grooming episodes in hM3D-expressing animals following saline or CNO administration. (K) Duration of social interaction in EYFP or hM3D-expressing animals following saline or CNO administration. (K) n = 8 animals for both hM3D and EYFP control.

Data are mean ± SEM. **p < 0.01, ***p < 0.001. See also Figure S6.

trials (Figures 6A–6E). Similarly, optogenetic activation of these glutamatergic neurons also suppressed naturally occurring mounting behavior toward a female (Figures 6A and 6F–6H).

The suppression of social behaviors by glutamatergic neurons could be explained by two alternative hypotheses: (1) simple physical incompatibility with evoked self-grooming behavior that dominates spontaneous social behavior (Figure 6I, upper), or (2) direct inhibition of social behaviors that is not causally related to the promotion of self-grooming (Figure 6I, lower). During stimulation of vGLUT2⁺ neurons, the interruption of ongoing attack occurred prior to the onset of self-grooming, with an average delay of 4.6 ± 0.8 s; a similar average delay of

5.3 ± 0.6 s was observed for the interruption of mounting (Figure 6J). Thus, the interruption of ongoing social behavior preceded the onset of self-grooming following activation of glutamatergic neurons, arguing that these neurons independently suppress social behavior.

To investigate this issue further, we performed long-term pharmacogenetic activation of vGLUT2$^+$ neurons in MeApd using a Cre-dependent virus encoding the activating DREADD hM3D and an mCherry fluorescent marker (Alexander et al., 2009) (Figure 6L). Successful pharmacogenetic activation of vGLUT2$^+$ neurons via injection of the specific ligand CNO was confirmed by double labeling for mCherry and c-*fos* (Figure S6A–S6B). Interestingly, pharmacogenetic activation of vGLUT2$^+$ neurons resulted in a marked reduction of social interactions (from ~400 s to ~200 s) (Figures 6K, 6M, and 6N). In contrast, this manipulation did not reduce interactions with novel objects (Figure S6D), suggesting that it did not promote a state of anxiety. Importantly, under these conditions, self-grooming was only sporadically evoked and occupied only ~20 s of the total observation period (12 min; Figure S6C), which cannot account for the duration and total extent of reduced social interactions. These data demonstrate that activation of vGLUT2$^+$ neurons in MeApd causes an active suppression of social interactions, independently of its effect to promote self-grooming behavior. Together, the foregoing results indicate that GABAergic and glutamatergic neurons in MeApd exert antagonistic influences to promote and inhibit social behaviors, respectively.

GABAergic Neurons Suppress Naturally Occurring Self Grooming

The observation that MeApd glutamatergic neurons actively inhibit social behaviors prompted us to ask whether activation of the vGAT$^+$ population might, conversely, inhibit self-grooming behavior. Indeed, optogenetic activation of vGAT$^+$ neurons acutely interrupted ongoing, spontaneous self-grooming behavior (Figure 7A; Movie S6), in a manner time-locked to the onset of photostimulation. This suppression could reflect (1) an indirect inhibition due to promotion of attack (Figure 7B, upper), or (2) a parallel influence to inhibit self-grooming that is independent of the promotion of social behavior (Figure 7B, lower).

To distinguish between these possibilities, we optogenetically activated MeApd vGAT$^+$ neurons in solitary animals in their home cage. Under these conditions, photostimulation-dependent suppression of self-grooming was observed in animals performing spontaneous bouts of self-grooming (Figures 7A and 7C). Self-grooming was interrupted in <2 s following the onset of stimulation in over 95% of trials (Figures 7C–7F). This interruption of grooming was not observed in EYFP-expressing animals (Figures 7A and 7D–7F). Because no intruder animal was present in the cage, this inhibition of self-grooming cannot be explained by physical incompatibility with social behaviors promoted by vGAT$^+$ neuron activation. Thus, our evidence indicates that MeApd GABAergic neurons exert an influence to suppress self-grooming, independently of their function to promote social behaviors.

To examine whether activation of MeApd vGAT$^+$ neurons might generally suppress any nonsocial goal-oriented behavior, we also investigated the influence of vGAT$^+$ neurons on feeding behavior. Optogenetic activation of vGAT$^+$ neurons did not inhibit ongoing feeding behavior (Figures 7G–7K). Although we cannot exclude that other solitary behaviors might be inhibited by GABAergic neuron activation, at the very least these data indicate that vGAT$^+$ neurons do not suppress any type of nonsocial behavior, suggesting a specific inhibitory influence on self-grooming.

DISCUSSION

Using cell-type-specific functional manipulations, we identified two nonoverlapping neuronal subpopulations in MeApd that promote social and nonsocial behaviors. GABAergic MeApd neurons promoted three different social behaviors in an intensity-dependent manner: aggression, mounting, and social grooming. In contrast, neighboring glutamatergic neurons in MeApd and adjacent LHA promoted repetitive self-grooming, an asocial behavior. This glutamatergic subpopulation also inhibited social behaviors, independently of its effect to promote self-grooming. Conversely, MeApd GABAergic neurons suppressed self-grooming, in both paired and solitary animals. Together, these data suggest that inhibitory and excitatory MeApd subpopulations control social behaviors versus repetitive self-grooming, respectively, in an antagonistic manner. These data provide insights into the circuit-level control of opponent innate behaviors by the MeA.

MeApd GABAergic Neurons Promote Aggression

The MeA is activated by chemosensory cues and relays this information through complex circuitry that involves connections with the bed nucleus of the stria terminalis (BNST) and the medial hypothalamus (Choi et al., 2005; Dong et al., 2001; Swanson, 2000). It has been proposed, based on c-*fos* activation and lesion studies, that this circuit is subdivided into topographically segregated pathways that control defensive versus reproductive (sexual) behaviors (Canteras et al., 1995; Swanson, 2000). According to this hodological scheme, MeApd is associated with reproductive behaviors and MeApv with defensive behaviors.

How the control of aggression fits into this scheme has not been clear, as aggression has both defensive and offensive forms (Blanchard et al., 2003). Our data provide definitive evidence that MeApd activity is both necessary and sufficient for intermale offensive aggression. Our data further demonstrate that the aggression-promoting neurons in MeApd are GABAergic, while glutamatergic neurons inhibit aggression. These data may explain in part why previous lesion studies of MeA have yielded contradictory results (Busch and Barfield, 1974; Kemble et al., 1984; Rosvold et al., 1954; Takahashi and Gladstone, 1988; Vochteloo and Koolhaas, 1987; Wang et al., 2013). Because VMHvl attack neurons are likely glutamatergic (Choi et al., 2005; Lin et al., 2011), it seems probable that MeApd GABAergic neurons promote aggression via disinhibition of these glutamatergic neurons. Functional studies will be required to identify potential disinhibition site(s).

Scalable Control of Social Behaviors in MeApd

Recent studies have revealed that Esr1$^+$ neurons in VMHvl (also expressing the progesterone receptor) (Yang et al., 2013)

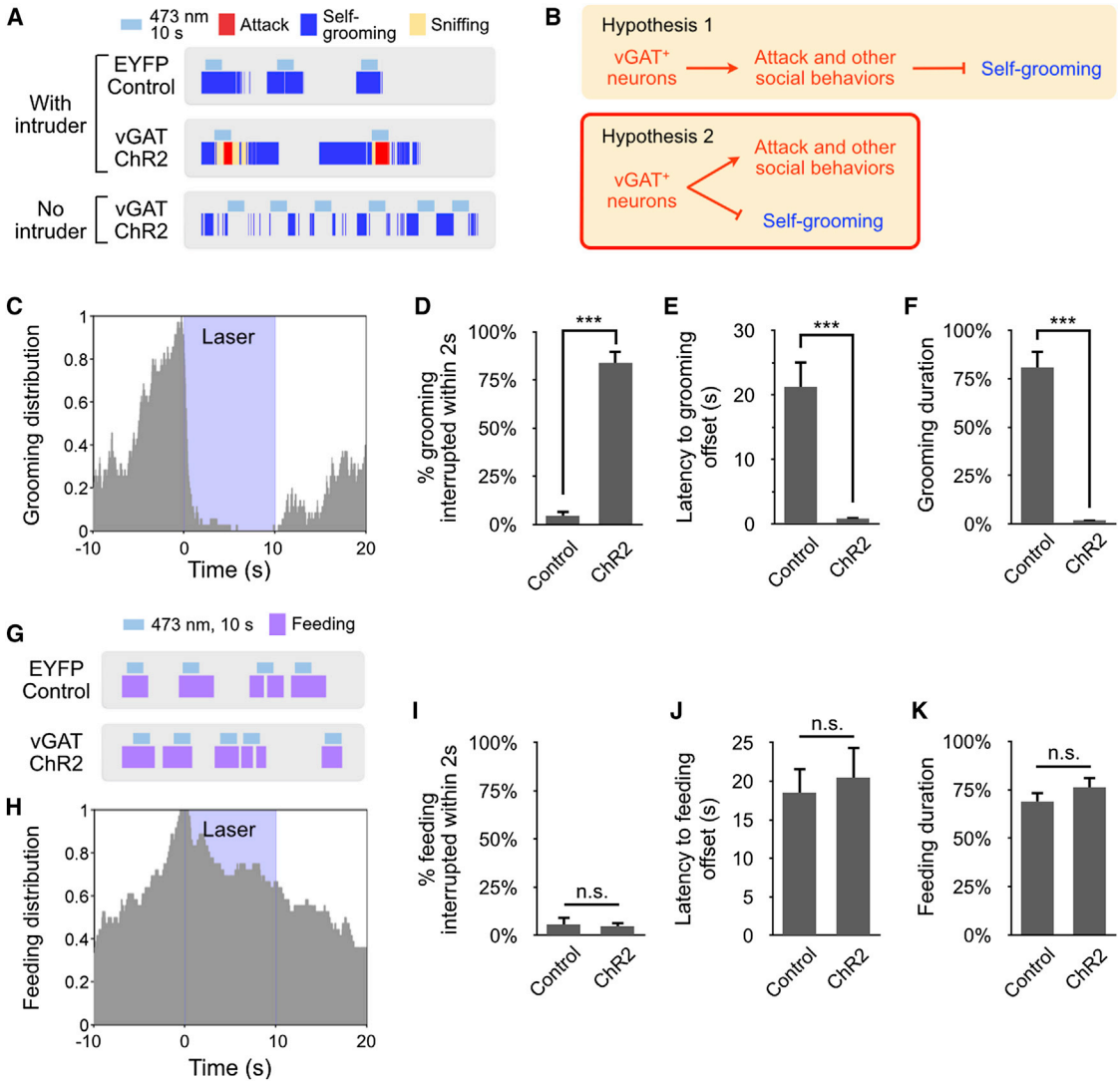

Figure 7. vGAT$^+$ Neurons Suppress Naturally Occurring Self-Grooming Behavior

(A–F) ChR2 activation of vGAT$^+$ neurons in MeApd suppresses ongoing self-grooming behavior. (A) Representative raster plots illustrating sniffing, attack and self-grooming behavior episodes in the presence or absence of intact BALB/c intruder males. (B) Two alternative hypotheses of how vGAT$^+$ neurons suppress self-grooming. (C) Distribution of self-grooming episodes (percentage of trials showing self-grooming at different time points) with respect to the initiation of laser illumination in ChR2-expressing males. (D) Percentage of self-grooming episodes interrupted within two seconds after the initiation of the laser illumination. (E) Latency to stop self-grooming with respect to the initiation of the laser illumination. (F) Percentage of time spent self-grooming during the 15 s photostimulation period. In (C)–(F), optogenetic stimulations are applied to solitary animals. (C–F), n = 100 trials for ChR2 experiment, n = 50 trials for control.

(G–K) ChR2 activation of vGAT$^+$ neurons in MeApd does not suppress ongoing feeding behavior. (G) Representative raster plots illustrating feeding episodes in the absence of intruders. (H) Distribution of feeding episodes with respect to the initiation of laser illumination in ChR2-expressing males. (I) Percentage of feeding episodes interrupted within two seconds after the initiation of the laser illumination. (J) Latency to stop feeding with respect to the initiation of the laser illumination. (K) Percentage of time spent feeding during the 15 s photostimulation period. (H–K), n = 36 trials for each condition.

Data are mean ± SEM. n.s., $p > 0.05$, ***$p < 0.001$. See also Figure S7 and Movie S6.

control multiple social behaviors in an intensity-dependent manner: stronger optogenetic stimulation evokes attack whereas weaker optogenetic stimulation elicits social investigation and mounting (Lee et al., 2014). Our finding that vGAT$^+$ neurons in MeApd control multiple social behaviors in a scalable manner echoes these observations and suggests that this scalable control of social behavior may already emerge at the level of MeApd. Alternatively, it may reflect feedback from VMHvl (Canteras et al., 1994). Several models can explain how such an intensity coding of social behavior is implemented at the cellular level, including different populations of neurons with different activation thresholds, or graded changes in activity within a single population (Lee et al., 2014). Distinguishing between these mechanisms, and the locations(s) at which they are implemented, will be an important topic for future investigation.

Antagonistic Control of Self-Grooming and Social Behaviors in MeApd

It is striking that MeA neurons that promote self-grooming can be cleanly separated from those that promote social behaviors, along the axis of excitatory versus inhibitory neurons, respectively. Self-grooming has traditionally been associated with the paraventricular hypothalamic nucleus, which is distinct from regions that control social behaviors (Kruk et al., 1998). Self-grooming can be observed in a variety of contexts and may express different internal states of either positive or negative valence (Tinbergen, 1951). The internal drives or motivations associated with the repetitive self-grooming elicited in these experiments are not clear and could reflect anxiogenic, anxiolytic, social avoidance or other states. The fact that activation of vGLUT2^{+} neurons in MeApd and adjacent LHA elicits self-grooming, but not other activities such as feeding, drinking, freezing, flight, digging or nesting, suggests that the influence of these neurons is specific for this repetitive asocial behavior.

Our experiments further reveal that these two MeA subpopulations not only control self-grooming and social behavior in a mutually exclusive and positive-acting manner, but that they also each play a negative-acting role to inhibit the behavior promoted by the other: the GABAergic neurons inhibit self-grooming, while the glutamatergic neurons inhibit social behaviors (Figure S7). Importantly, the observed reciprocal inhibitory effects do not reflect simple physical incompatibility between behaviors promoted in a positive-acting manner, but rather reflect an independent, negative-acting function for both neuronal subpopulations. Identification of the site(s) and synaptic mechanisms underlying such reciprocal antagonism will be an important topic for future study.

Potential Relevance to Psychiatric Disorders Affecting Social Interactions

Abnormalities in social behaviors have been observed in several psychiatric disorders, including autism and schizophrenia (Couture et al., 2010; Sasson et al., 2007). Impaired social interactions are a major symptom of autism, for example, and are a signature phenotype in many mouse models of this disorder (Silverman et al., 2010; Williams, 2008). A prominent hypothesis, the "excitation:inhibition imbalance hypothesis," posits that autism may be caused by an increase in the relative level of excitation versus inhibition in multiple brain regions (Markram and Markram, 2010; Rubenstein and Merzenich, 2003). In that context, it is striking that social interactions were strongly inhibited by increasing the level of excitatory neuronal activity in the amygdala, a structure whose dysfunction has been implicated in autism (Baron-Cohen et al., 2000; Birmingham et al., 2011). Such manipulations, moreover, also promoted repetitive self-grooming, a behavioral phenotype seen in some genetic mouse models of autism as well (Blundell et al., 2010; Etherton et al., 2009; Silverman et al., 2010). Conversely, activation of amygdala GABAergic neurons promoted social behaviors and inhibited self-grooming. These unexpected findings suggest that this system may prove useful for investigating further how alterations in the relative levels of excitatory versus inhibitory neuronal activity in the amygdala can influence the "decision" to engage in social versus repetitive asocial behaviors. They may also suggest candidate neural substrates for gene variants implicated in psychiatric disorders that affect social interactions in humans (Fatemi et al., 2002; Jamain et al., 2002).

EXPERIMENTAL PROCEDURES

Experimental Subjects

Subjects were wild-type C57BL/6N (Charles River), vGAT$^{Cre/+}$, or vGLUT2$^{Cre/+}$ male mice (Vong et al., 2011). Intruder mice were BALB/c or C57BL/6N males (intact and castrated) and BALB/c females, purchased at 8 weeks old (Charles River). Care and experimental manipulations of animals were in accordance with the NIH Guide for Care and Use of Laboratory Animals and approved by the Caltech Institutional Animal Care and Use Committee.

Stereotaxic Surgery, Virus Injection, and Optic-Fiber Placement

Mice at 8 weeks old were anesthetized with isoflurane and mounted in a stereotaxic apparatus (Kopf Instruments). In all experiments except for Figure S5, viruses were injected bilaterally into MeApd (ML ±2.00, AP −1.50, DV −5.15 from bregma). In Figure S5, viruses were injected using slightly different stereotaxic coordinates along the mediolateral axis (ML between ±1.60 and ±2.10, AP −1.50, DV −5.15 from bregma). Injections were carried out using a pulled, fine glass capillary at a rate of 30 nl min^{-1} for a total volume of 300 nl. A custom made ferrule fiber (200 μm in core diameter, Doric Lenses) was subsequently placed at 0.5 mm above the virus injection site in the target brain area and fixed on the skull with dental cement (Parkell; Metabond). In all experiments the virus was allowed 3–4 weeks to incubate before behavioral testing or perfusion. Unless otherwise indicated, all control animals used in this study were animals with the same genetic background injected with viruses expressing EYFP.

Optogenetic Activation and Silencing

Wild-type, vGAT$^{Cre/+}$, or vGLUT2$^{Cre/+}$ mice at 8 weeks old were injected bilaterally into MeApd with a rAAV expressing ChR2 or eNpHR3 and bilaterally implanted with optic fibers. After a 3–4 week recovery period, the virus-injected animals were subject to behavioral testing in their home cage for 2 to 4 weeks. Photostimulation (ChR2, 473 nm, 20 Hz, 20 ms pulses, 1–3 mW mm^{-2}; or eNpHR3, 593 nm, continuous, 1–3 mW mm^{-2}) was administered to mice in the absence or presence of an intruder mouse.

Pharmacogenetic Activation

vGLUT2$^{Cre/+}$ mice at 8 weeks old were injected bilaterally into MeApd with a Cre-dependent rAAV expressing the pharmacogenetic activator DREADD hM3D (AAV2-EF1α-DIO-hM3D-mCherry). The virus was allowed 4 weeks to incubate before behavioral testing. CNO (Clozapine N-oxide, 1.5 mg/kg, Enzo Life Sciences) or saline was administrated by intraperitoneal injection. Thirty minutes after the CNO or saline administration, animals were transferred in their home cage to a behavioral testing room and were tested for social interaction and self-grooming.

Behavioral Testing

Aggression was examined using the resident-intruder assay. Housing conditions prior to surgery were selected depending on the level of baseline aggression appropriate for activation (low baseline) versus inhibition (high baseline) experiments. A more submissive mouse was used as the intruder male in all the experiments; all resident animals included in the study initiated all the attacks during the aggression test. See Extended Experimental Procedures for additional behavioral tests.

Additional Methods

Detailed methods on experimental subjects, viral vectors, behavioral assays, behavior equipment setup, video acquisition and analysis, optogenetic stimulation, acute slice electrophysiology, and immunohistochemistry can be found in the Extended Experimental Procedures.

SUPPLEMENTAL INFORMATION

Supplemental Information includes Extended Experimental Procedures, seven figures, and six movies and can be found with this article online at http://dx.doi.org/10.1016/j.cell.2014.07.049.

AUTHOR CONTRIBUTIONS

W.H. and D.J.A. designed the experiments. W.H. performed most of the experiments. D.-W.K. performed electrophysiological recordings. D.J.A. supervised the project. W.H. and D.J.A wrote the manuscript.

ACKNOWLEDGMENTS

We thank X. Wang, X. Da, M. McCardle, R. Robertson, and C. Park for technical assistance, T. Anthony for the ChR2 virus, the Caltech GEMS and animal facility for maintaining mice, M. Zelikowsky, H. Cai, and K. Asahina for commenting on the manuscript, and members of the D.J.A. laboratory for discussions. W.H. is a Helen Hey Whitney Fellow. D.J.A. is a Howard Hughes Medical Institute Investigator and a Paul G. Allen Distinguished Investigator. This work was supported in part by NIH grants MH085082 and MH070053, and a grant from Gerald Fischbach and the Simons Foundation.

Received: March 4, 2014
Revised: May 27, 2014
Accepted: July 17, 2014
Published: September 11, 2014

REFERENCES

Adams, D.B. (2006). Brain mechanisms of aggressive behavior: an updated review. Neurosci. Biobehav. Rev. *30*, 304–318.

Alexander, G.M., Rogan, S.C., Abbas, A.I., Armbruster, B.N., Pei, Y., Allen, J.A., Nonneman, R.J., Hartmann, J., Moy, S.S., Nicolelis, M.A., et al. (2009). Remote control of neuronal activity in transgenic mice expressing evolved G protein-coupled receptors. Neuron *63*, 27–39.

Aravanis, A.M., Wang, L.-P., Zhang, F., Meltzer, L.A., Mogri, M.Z., Schneider, M.B., and Deisseroth, K. (2007). An optical neural interface: in vivo control of rodent motor cortex with integrated fiberoptic and optogenetic technology. J. Neural Eng. *4*, S143–S156.

Baron-Cohen, S., Ring, H.A., Bullmore, E.T., Wheelwright, S., Ashwin, C., and Williams, S.C. (2000). The amygdala theory of autism. Neurosci. Biobehav. Rev. *24*, 355–364.

Bergan, J.F., Ben-Shaul, Y., and Dulac, C. (2014). Sex-specific processing of social cues in the medial amygdala. eLife *3*, e02743.

Bian, X., Yanagawa, Y., Chen, W.R., and Luo, M. (2008). Cortical-like functional organization of the pheromone-processing circuits in the medial amygdala. J. Neurophysiol. *99*, 77–86.

Birmingham, E., Cerf, M., and Adolphs, R. (2011). Comparing social attention in autism and amygdala lesions: effects of stimulus and task condition. Soc. Neurosci. *6*, 420–435.

Blanchard, R.J., Wall, P.M., and Blanchard, D.C. (2003). Problems in the study of rodent aggression. Horm. Behav. *44*, 161–170.

Blundell, J., Blaiss, C.A., Etherton, M.R., Espinosa, F., Tabuchi, K., Walz, C., Bolliger, M.F., Südhof, T.C., and Powell, C.M. (2010). Neuroligin-1 deletion results in impaired spatial memory and increased repetitive behavior. J. Neurosci. *30*, 2115–2129.

Boyden, E.S., Zhang, F., Bamberg, E., Nagel, G., and Deisseroth, K. (2005). Millisecond-timescale, genetically targeted optical control of neural activity. Nat. Neurosci. *8*, 1263–1268.

Busch, D.E., and Barfield, R.J. (1974). A failure of amygdaloid lesions to alter agonistic behavior in the laboratory rat. Physiol. Behav. *12*, 887–892.

Canteras, N.S., Simerly, R.B., and Swanson, L.W. (1994). Organization of projections from the ventromedial nucleus of the hypothalamus: a Phaseolus vulgaris-leucoagglutinin study in the rat. J. Comp. Neurol. *348*, 41–79.

Canteras, N.S., Simerly, R.B., and Swanson, L.W. (1995). Organization of projections from the medial nucleus of the amygdala: a PHAL study in the rat. J. Comp. Neurol. *360*, 213–245.

Chamero, P., Marton, T.F., Logan, D.W., Flanagan, K., Cruz, J.R., Saghatelian, A., Cravatt, B.F., and Stowers, L. (2007). Identification of protein pheromones that promote aggressive behaviour. Nature *450*, 899–902.

Choi, G.B., Dong, H.-W., Murphy, A.J., Valenzuela, D.M., Yancopoulos, G.D., Swanson, L.W., and Anderson, D.J. (2005). Lhx6 delineates a pathway mediating innate reproductive behaviors from the amygdala to the hypothalamus. Neuron *46*, 647–660.

Couture, S.M., Penn, D.L., Losh, M., Adolphs, R., Hurley, R., and Piven, J. (2010). Comparison of social cognitive functioning in schizophrenia and high functioning autism: more convergence than divergence. Psychol. Med. *40*, 569–579.

Dhungel, S., Masaoka, M., Rai, D., Kondo, Y., and Sakuma, Y. (2011). Both olfactory epithelial and vomeronasal inputs are essential for activation of the medial amygdala and preoptic neurons of male rats. Neuroscience *199*, 225–234.

Dong, H.W., Petrovich, G.D., and Swanson, L.W. (2001). Topography of projections from amygdala to bed nuclei of the stria terminalis. Brain Res. Brain Res. Rev. *38*, 192–246.

Dulac, C., and Torello, A.T. (2003). Molecular detection of pheromone signals in mammals: from genes to behaviour. Nat. Rev. Neurosci. *4*, 551–562.

Duvarci, S., and Pare, D. (2014). Amygdala microcircuits controlling learned fear. Neuron *82*, 966–980.

Ehrlich, I., Humeau, Y., Grenier, F., Ciocchi, S., Herry, C., and Lüthi, A. (2009). Amygdala inhibitory circuits and the control of fear memory. Neuron *62*, 757–771.

Erskine, M.S. (1993). Mating-induced increases in FOS protein in preoptic area and medial amygdala of cycling female rats. Brain Res. Bull. *32*, 447–451.

Etherton, M.R., Blaiss, C.A., Powell, C.M., and Südhof, T.C. (2009). Mouse neurexin-1alpha deletion causes correlated electrophysiological and behavioral changes consistent with cognitive impairments. Proc. Natl. Acad. Sci. USA *106*, 17998–18003.

Fatemi, S.H., Halt, A.R., Stary, J.M., Kanodia, R., Schulz, S.C., and Realmuto, G.R. (2002). Glutamic acid decarboxylase 65 and 67 kDa proteins are reduced in autistic parietal and cerebellar cortices. Biol. Psychiatry *52*, 805–810.

Gradinaru, V., Zhang, F., Ramakrishnan, C., Mattis, J., Prakash, R., Diester, I., Goshen, I., Thompson, K.R., and Deisseroth, K. (2010). Molecular and cellular approaches for diversifying and extending optogenetics. Cell *141*, 154–165.

Jamain, S., Betancur, C., Quach, H., Philippe, A., Fellous, M., Giros, B., Gillberg, C., Leboyer, M., and Bourgeron, T.; Paris Autism Research International Sibpair (PARIS) Study (2002). Linkage and association of the glutamate receptor 6 gene with autism. Mol. Psychiatry *7*, 302–310.

Kemble, E.D., Blanchard, D.C., Blanchard, R.J., and Takushi, R. (1984). Taming in wild rats following medial amygdaloid lesions. Physiol. Behav. *32*, 131–134.

Kollack, S.S., and Newman, S.W. (1992). Mating behavior induces selective expression of Fos protein within the chemosensory pathways of the male Syrian hamster brain. Neurosci. Lett. *143*, 223–228.

Kollack-Walker, S., and Newman, S.W. (1995). Mating and agonistic behavior produce different patterns of Fos immunolabeling in the male Syrian hamster brain. Neuroscience *66*, 721–736.

Kondo, Y. (1992). Lesions of the medial amygdala produce severe impairment of copulatory behavior in sexually inexperienced male rats. Physiol. Behav. *51*, 939–943.

Kondo, Y., and Arai, Y. (1995). Functional association between the medial amygdala and the medial preoptic area in regulation of mating behavior in the male rat. Physiol. Behav. *57*, 69–73.

Kruk, M.R. (1991). Ethology and pharmacology of hypothalamic aggression in the rat. Neurosci. Biobehav. Rev. *15*, 527–538.

Kruk, M.R., Westphal, K.G., Van Erp, A.M., van Asperen, J., Cave, B.J., Slater, E., de Koning, J., and Haller, J. (1998). The hypothalamus: cross-roads of endocrine and behavioural regulation in grooming and aggression. Neurosci. Biobehav. Rev. *23*, 163–177.

Lee, H., Kim, D.-W., Remedios, R., Anthony, T.E., Chang, A., Madisen, L., Zeng, H., and Anderson, D.J. (2014). Scalable control of mounting and attack by Esr1+ neurons in the ventromedial hypothalamus. Nature *509*, 627–632.

Lehman, M.N., Winans, S.S., and Powers, J.B. (1980). Medial nucleus of the amygdala mediates chemosensory control of male hamster sexual behavior. Science *210*, 557–560.

Lin, D., Boyle, M.P., Dollar, P., Lee, H., Lein, E.S., Perona, P., and Anderson, D.J. (2011). Functional identification of an aggression locus in the mouse hypothalamus. Nature *470*, 221–226.

Madisen, L., Zwingman, T.A., Sunkin, S.M., Oh, S.W., Zariwala, H.A., Gu, H., Ng, L.L., Palmiter, R.D., Hawrylycz, M.J., Jones, A.R., et al. (2010). A robust and high-throughput Cre reporting and characterization system for the whole mouse brain. Nat. Neurosci. *13*, 133–140.

Mandiyan, V.S., Coats, J.K., and Shah, N.M. (2005). Deficits in sexual and aggressive behaviors in Cnga2 mutant mice. Nat. Neurosci. *8*, 1660–1662.

Markram, K., and Markram, H. (2010). The intense world theory - a unifying theory of the neurobiology of autism. Front. Hum. Neurosci. *4*, 224.

Nelson, R.J., and Trainor, B.C. (2007). Neural mechanisms of aggression. Nat. Rev. Neurosci. *8*, 536–546.

Newman, S.W. (1999). The medial extended amygdala in male reproductive behavior. A node in the mammalian social behavior network. Ann. N Y Acad. Sci. *877*, 242–257.

Niimi, K., Horie, S., Yokosuka, M., Kawakami-Mori, F., Tanaka, K., Fukayama, H., and Sahara, Y. (2012). Heterogeneous electrophysiological and morphological properties of neurons in the mouse medial amygdala in vitro. Brain Res. *1480*, 41–52.

Paré, D., Quirk, G.J., and Ledoux, J.E. (2004). New vistas on amygdala networks in conditioned fear. J. Neurophysiol. *92*, 1–9.

Pitkänen, A., Savander, V., and LeDoux, J.E. (1997). Organization of intra-amygdaloid circuitries in the rat: an emerging framework for understanding functions of the amygdala. Trends Neurosci. *20*, 517–523.

Rosvold, H.E., Mirsky, A.F., and Pribram, K.H. (1954). Influence of amygdalectomy on social behavior in monkeys. J. Comp. Physiol. Psychol. *47*, 173–178.

Rubenstein, J.L.R., and Merzenich, M.M. (2003). Model of autism: increased ratio of excitation/inhibition in key neural systems. Genes Brain Behav. *2*, 255–267.

Sasson, N., Tsuchiya, N., Hurley, R., Couture, S.M., Penn, D.L., Adolphs, R., and Piven, J. (2007). Orienting to social stimuli differentiates social cognitive impairment in autism and schizophrenia. Neuropsychologia *45*, 2580–2588.

Siegel, A., Roeling, T.A., Gregg, T.R., and Kruk, M.R. (1999). Neuropharmacology of brain-stimulation-evoked aggression. Neurosci. Biobehav. Rev. *23*, 359–389.

Silverman, J.L., Yang, M., Lord, C., and Crawley, J.N. (2010). Behavioural phenotyping assays for mouse models of autism. Nat. Rev. Neurosci. *11*, 490–502.

Stanley, D.A., and Adolphs, R. (2013). Toward a neural basis for social behavior. Neuron *80*, 816–826.

Stowers, L., Holy, T.E., Meister, M., Dulac, C., and Koentges, G. (2002). Loss of sex discrimination and male-male aggression in mice deficient for TRP2. Science *295*, 1493–1500.

Swanson, L.W. (2000). Cerebral hemisphere regulation of motivated behavior. Brain Res. *886*, 113–164.

Swanson, L.W., and Petrovich, G.D. (1998). What is the amygdala? Trends Neurosci. *21*, 323–331.

Takahashi, L.K., and Gladstone, C.D. (1988). Medial amygdaloid lesions and the regulation of sociosexual behavioral patterns across the estrous cycle in female golden hamsters. Behav. Neurosci. *102*, 268–275.

Tinbergen, N. (1951). The Study of Instinct (New York, NY: Clarendon Press/Oxford University Press).

Veening, J.G., Coolen, L.M., de Jong, T.R., Joosten, H.W., de Boer, S.F., Koolhaas, J.M., and Olivier, B. (2005). Do similar neural systems subserve aggressive and sexual behaviour in male rats? Insights from c-Fos and pharmacological studies. Eur. J. Pharmacol. *526*, 226–239.

Vochteloo, J.D., and Koolhaas, J.M. (1987). Medial amygdala lesions in male rats reduce aggressive behavior: interference with experience. Physiol. Behav. *41*, 99–102.

Vong, L., Ye, C., Yang, Z., Choi, B., Chua, S., Jr., and Lowell, B.B. (2011). Leptin action on GABAergic neurons prevents obesity and reduces inhibitory tone to POMC neurons. Neuron *71*, 142–154.

Wang, Y., He, Z., Zhao, C., and Li, L. (2013). Medial amygdala lesions modify aggressive behavior and immediate early gene expression in oxytocin and vasopressin neurons during intermale exposure. Behav. Brain Res. *245*, 42–49.

Williams, J.H. (2008). Self-other relations in social development and autism: multiple roles for mirror neurons and other brain bases. Autism Res. *1*, 73–90.

Xu, X., Coats, J.K., Yang, C.F., Wang, A., Ahmed, O.M., Alvarado, M., Izumi, T., and Shah, N.M. (2012). Modular genetic control of sexually dimorphic behaviors. Cell *148*, 596–607.

Yang, C.F., Chiang, M.C., Gray, D.C., Prabhakaran, M., Alvarado, M., Juntti, S.A., Unger, E.K., Wells, J.A., and Shah, N.M. (2013). Sexually dimorphic neurons in the ventromedial hypothalamus govern mating in both sexes and aggression in males. Cell *153*, 896–909.

Yoon, H., Enquist, L.W., and Dulac, C. (2005). Olfactory inputs to hypothalamic neurons controlling reproduction and fertility. Cell *123*, 669–682.

Zufall, F., and Leinders-Zufall, T. (2007). Mammalian pheromone sensing. Curr. Opin. Neurobiol. *17*, 483–489.

Cell

EXTENDED EXPERIMENTAL PROCEDURES

Experimental Subjects

Eight-week old male, female, and castrated male mice of C57BL/6N and BALB/c backgrounds were purchased from Charles Rivers Laboratory. vGAT-ires-Cre and vGLUT2-ires-Cre knockin animals (Vong et al., 2011) were initially purchased from Jackson Laboratories and then backcrossed to the C57BL/6N background in the Caltech animal facility. The Ai6 reporter line, Rosa-LSL-ZsGreen (Madisen et al., 2010), was obtained from the Allen Institute of Brain Science. Animals were housed and maintained on a reversed 12-h light-dark cycle for at least one week prior to stereotaxic surgery or behavioral testing. All the control experiments were done using animals with the same genetic background. Care and experimental manipulations of animals were in accordance with the National Institute of Health Guide for Care and Use of Laboratory Animals and approved by the Caltech Institutional Animal Care and Use Committee.

Viral Vectors

AAV2-CMV-Cre was purchased from Vector Laboratories. AAV2-EF1α-DIO-mCherry, AAV2-EF1α-DIO-EYFP, AAV2-EF1α-DIO-ChR2-mCherry, AAV2-EF1α-DIO-eNpHR3-mCherry, AAV2-EF1α-DIO-eNpHR3-EYFP, and AAV2-EF1α-DIO-hM3D-mCherry were purchased from the University of North Carolina vector core facility. AAV2-EF1α-FLEX-ChR2-nuclear hrGFP (Lee et al., 2014) was produced by University of Pennsylvania vector core facility.

Behavioral Assay for Aggression

Aggression was examined using the resident-intruder assay (Blanchard et al., 2003). Resident males were transferred in their home cage to a behavioral testing room containing a customized behavioral chamber equipped with video acquisition capabilities (see below). An unfamiliar male (“intruder”) mouse was then introduced into the home cage of the tested resident. The resident and intruder were allowed to interact with each other freely for 15∼60 min before the intruder was removed. If excessive tissue damage was observed consequent to fighting, the interaction was terminated prematurely. In c-*fos* induction experiments in Figures 1A–1D and 2A–2E, the resident mice were sacrificed 1 hr after the intruder was removed, and their brains were collected for anatomical studies to map the neurons that have been active during the aggression assay.

Housing conditions prior to surgery were selected depending on the level of baseline aggression appropriate for activation (low baseline) versus inhibition (high baseline) experiments. Early social isolation increases aggression, while group housing suppresses it (Koike et al., 2009; Tóth et al., 2008). Therefore, to decrease baseline aggression in experiments designed to analyze optogenetic activation of attack, both control and opsin-expressing animals were group-housed prior to surgery. Conversely, to increase baseline aggression in experiments designed to analyze optogenetic inhibition of attack, both control and opsin-expressing animals were housed in social isolation for 4 weeks prior to surgery. Because there is animal-to-animal variability in baseline aggression levels, even when group housing versus social isolation conditions are used, implanted control and opsin-expressing animals were prescreened for baseline levels of aggression prior to extensive testing. Animals showing high levels of baseline aggression despite group housing (∼5% of the total animals; “high levels” defined as exhibiting attacks during > 40% of the total experiment duration), and animals showing low levels of baseline aggression despite social isolation (∼20% of the total animals; “low levels” defined as exhibiting attacks during < 3% of the experiment duration), were eliminated from further analysis.

The resident-intruder assay used in this study was designed to study offensive aggression. To avoid intruder-initiated aggression, all intruder animals were group housed to reduce their aggression level. A more submissive mouse strain BALB/c or a prescreened, nonaggressive C57BL/6N were used as the intruder male in all the experiments. All resident animals included in the study initiated all the attacks during the aggression test. In Figure 2S, an inanimate, stuffed toy mouse was used in place of an intruder. A new toy mouse was used for each test to avoid confounds due to residual odor from prior testing.

Behavior Assays for Mating, Self-Grooming, and Social Interactions

Mating was examined using the resident-intruder assay. Here, intact, nonhormone primed, group housed C57BL/6N female mice were used as intruder animals. A female mouse was allowed to interact with a male resident freely for 15∼60 min before she was removed.

Self-grooming behavior was examined either with the presence of an intruder animal in the resident-intruder assay or in solitary animals. Self-grooming behavior consists of a sequence of behaviors that proceed from paw licking to facial grooming and to body grooming (Movie S1). The self-grooming behavior evoked by optogenetic stimulation is similar to naturally occurring self-grooming behavior in wild-type animals.

Social interaction in Figures 6 and S6 was examined using a modified resident-intruder assay in which an unfamiliar target animal (intruder animal) is placed under an inverted pencil cup (Figure 6M). The resident animals were allowed to interact with the target animal freely for 15 min. Social interaction was defined as any sniffing and investigation behavior within 1 cm of the inverted pencil cup.

Behavior Equipment Setup, Video Acquisition, and Analysis

All behavioral assays were performed under infrared light conditions. To ensure the accurate scoring of various behaviors, and to minimize occlusion between mice, the sessions were recorded using a customized chamber with two synchronized infrared video

cameras placed at ninety-degree angles from each other (Figure S3). One camera (Basler 601f) was placed on top of the home cage, and the other (Basler 601f or Basler ace2000-50 gmNIR) placed in front of the cage. All videos were recorded at 30-50 fps. Two synchronized videos were annotated manually on a frame-by-frame basis using Piotr's MATLAB toolbox (http://vision.ucsd.edu/~pdollar/toolbox/doc/). Manual annotation was performed by an observer blind to experimental conditions. Annotations were then processed and analyzed using customized programs in MATLAB to characterize and quantify behavioral episodes.

Optogenetic Stimulation

Wild-type, $vGAT^{Cre/+}$, or $vGLUT2^{Cre/+}$ mice at 8 weeks old were injected bilaterally into MeApd with a rAAV expressing ChR2 or eNpHR3 and bilaterally implanted with optic fibers (ferrule fiber, Doric Lenses). After a 3–4-week recovery period, the virus-injected animals were subject to behavioral testing in their home cage for 2 to 4 weeks. Before behavioral testing, a ferrule patch cord was coupled to the ferrule fiber implanted in the mouse using a zirconia split sleeve (Doric Lenses) (Aravanis et al., 2007). Optic fibers were connected using an FC/PC adaptor (Doric Lenses) to a 473-nm blue laser or a 593-nm yellow laser (LaserGlow). Laser pulses were controlled through an Arduino micro-controller board and a customized MATLAB program. The MATLAB program sent commands through a serial connection to the Arduino micro-controller board, which in turn generated the TTL signals to the laser to produce illumination pulses. Stimulations were delivered based on resident mouse behavior, with an average of 10-20 stimulations per hour. Blue (473 nm) light was delivered in 20 ms pulses at 20 Hz, at final output powers ranging from 1–3 mW mm^{-2}. In Figure 4, a wider range of the laser output powers (0.5–5 mW mm^{-2}) were tested. Yellow (593 nm) light was delivered in a continuous pattern for 3 s, at final output powers ranging from 1–3 mW mm^{-2}. In Figures 1M, 2P, 3G, 3H, 5L, 5M, 6E, 7C and 7H, all trials were aligned to each other at indicated time points with respect to the onset of photostimulation. At each video frame, each trial was scored as showing the corresponding behavior or not. The percentage of all the trials showing the corresponding behavior during a given video frame was then plotted on the y axis on a scale of 0–1. In this way the average time of onset and offset as well as the duration of the corresponding behavior could be compared across trials.

To examine neuronal responses to the ChR2 activation in vivo, a train of blue light (473 nm, 30 s on and 30 s off, 20 ms, 20 Hz × 30) was delivered to induce c-*fos* expression in solitary animals (in the absence of any intruder animals). The animals were sacrificed an hour after the photostimulation. The animals had no contact with any other animals 48 hr prior to the c-*fos* induction experiment, to avoid any nonspecific induction of c-*fos* due to behavioral testing.

Acute Slice Electrophysiology

$vGAT^{Cre/+}$ or $vGLUT2^{Cre/+}$ males were injected into MeApd with a Cre-dependent AAV2 encoding ChR2-EYFP or a Cre-dependent AAV2 encoding eNpHR3.0-mCherry in a volume of 300 nl. After 3-4 weeks of viral incubation, coronal sections including the MeApd were cut at 300 μm using a vibratome (VT-1000S, Leica Microsystems) in ice-cold cutting solution. Slices were then incubated in artificial cerebrospinal fluid (ACSF) at 32°C for at least one hour, and recorded at room temperature (20-25°C). Cells expressing a virally encoded fluorescent marker (ChR2-EYFP and eNpHR3.0-mCherry) were visualized by infrared differential interference contrast (IR-DIC) and fluorescence video microscopy (Olympus BX51). Whole-cell current clamp recordings were performed with a MultiClamp 700B amplifier and Digidata 1440A (Molecular Devices). The patch clamp electrode (5-8 MΩ) was backfilled with an intracellular solution. Data were sampled at 10 kHz, filtered at 3 kHz, digitized and analyzed with pClamp10 software (Molecular Devices). Photostimulation (ChR2, 473 nm, 20 ms pulses; eNpHR3, 561 nm, continuous; CrystalLaser) was applied to the brain slices from the tip of an optical fiber. The spike fidelity in ChR2-expressing $vGAT^{+}$ or $vGLUT2^{+}$ neurons was measured by counting numbers of light pulses that successfully evoked action potentials upon 473 nm photostimulation (20 ms pulses) at different frequencies (2, 5, 10, 20, and 40 Hz).

Composition of solutions used in electrophysiology:

Cutting solution: 234 mM sucrose, 28 mM $NaHCO_3$, 7 mM dextrose, 2.5 mM KCl, 7 mM $MgCl_2$, 9.5 mM $CaCl_2$, 1 mM sodium ascorbate, 3 mM sodium pyruvate, and 1.25 mM NaH_2PO_4, oxygenated with 95% O_2/5% CO_2.

Artificial cerebrospinal fluid (ACSF): 119 mM NaCl, 25 mM $NaHCO_3$, 11 mM D-glucose, 2.5 mM KCl, 1.25 mM $MgCl_2$, 2 mM $CaCl_2$, 1.25 mM NaH_2PO_4, oxygenated with 95% O_2/5% CO_2.

Intracellular solution: 125 mM potassium gluconate, 10 mM KCl, 10 mM HEPES, 1 mM EGTA, 4 mM Mg-ATP, 0.3 mM Na_2GTP, and 10 mM sodium phosphocreatine, pH 7.25, 280-300 mOsm.

Immunohistochemistry

For immunofluorescence staining, mice were perfused transcardially with 4% paraformaldehyde in phosphate buffer. The brain was extracted and postfixed for 1 hr at room temperature, cryoprotected in 15% sucrose in PBS at 4°C, and frozen at −80°C. Sections 35 microns thick were cut on a cryostat (Leica Biosystems). Sections were either mounted onto superfrost slides for histological verification of injections or were cut free-floating and processed for c-*fos* staining. Tissue sections were blocked for 30 min at room temperature in PBS-T (0.1% Triton X-100) with 5% normal donkey serum, and stained with primary antibodies (overnight at 4°C) and secondary antibodies (2 hr at room temperature). Primary antibodies used were goat anti-c-*fos* (Santa Cruz Biotechnology, 1:200) and goat anti-V5 (Abcam ab9137, 1:400). Secondary antibody used was donkey anti-goat IgG Alexa 568 (Invitrogen, 1:500). Cell

bodies were identified using NeuroTrace 435/455 Blue Fluorescent Nissl stain (Invitrogen, 1:200), which was added during secondary antibody staining. Images are taken using multi-area stitching on a confocal microscope (Olympus FluoView FV1000); the boundary between two adjacent areas can sometimes be seen due to uneven illumination between tiles. Cell counting was carried out manually using ImageJ.

Statistical Analysis

Statistical analysis was performed using Prism 6 (GraphPad Software) and MATLAB (MathWorks). The data were analyzed using unpaired t test, Mann-Whitney U test, or Wilcoxon matched-pairs signed rank test. The cutoff for significance was held at $\alpha = 0.05$, two-tailed.

SUPPLEMENTAL REFERENCES

Koike, H., Ibi, D., Mizoguchi, H., Nagai, T., Nitta, A., Takuma, K., Nabeshima, T., Yoneda, Y., and Yamada, K. (2009). Behavioral abnormality and pharmacologic response in social isolation-reared mice. Behav. Brain Res. *202*, 114–121.

Tóth, M., Halász, J., Mikics, E., Barsy, B., and Haller, J. (2008). Early social deprivation induces disturbed social communication and violent aggression in adulthood. Behav. Neurosci. *122*, 849–854.

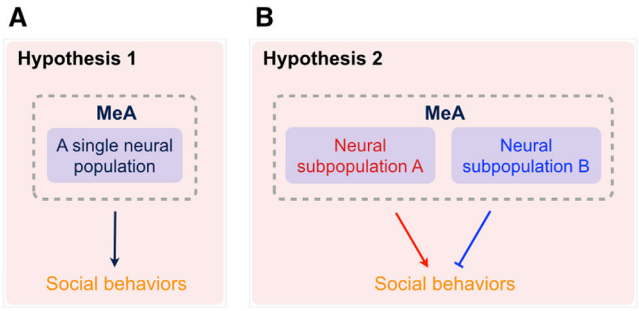

Figure S1. Summary of Two Alternative Hypotheses, Related to Figure 1
Two alternative hypotheses of how MeApd neurons control social behaviors.

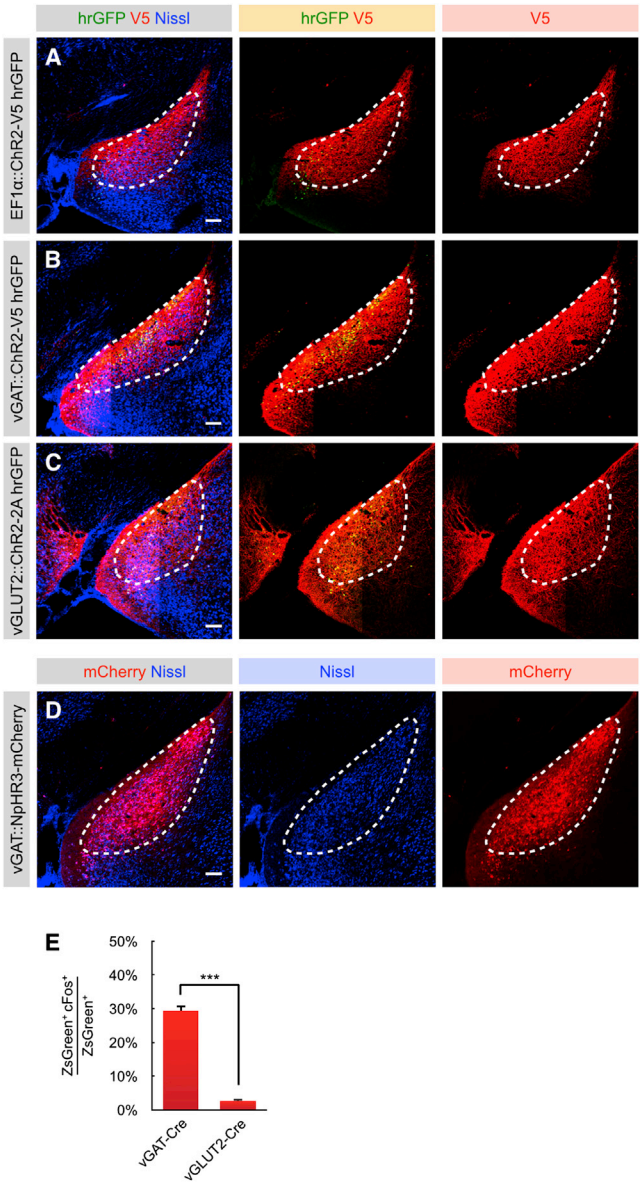

Figure S2. Viral Expression of ChR2 and eNpHR3 in MeApd, Related to Figures 1, 2, 3, and 5

(A–C) Representative images showing the expression of ChR2 by the viral vector AAV2-EF1α-FLEX-ChR2-nuclear hrGFP injected into MeApd. ChR2 is V5 epitope-tagged. Green, hrGFP native fluorescence; Red, V5 staining; blue, fluorescent Nissl stain. Scale bar: 50 μm.

(D) Representative images showing the expression of eNpHR3 by the viral vectors AAV2-EF1α-DIO-eNpHR3-mCherry injected into MeApd. eNpHR3 is tagged with mCherry. Images are taken using multi-area stitching on a confocal microscope; boundary between two adjacent areas can be seen due to uneven illumination. Red, mCherry native fluorescence; blue, fluorescent Nissl stain. Scale bar: 50 μm.

(E) Percentage of total ZsGreen^{+} cells that are c-*fos*$^{+}$ in vGAT$^{Cre/+}$ or vGLUT2$^{Cre/+}$ resident males following attack toward intruder males.

Data are mean ± SEM. ***p < 0.001 (Unpaired t test).

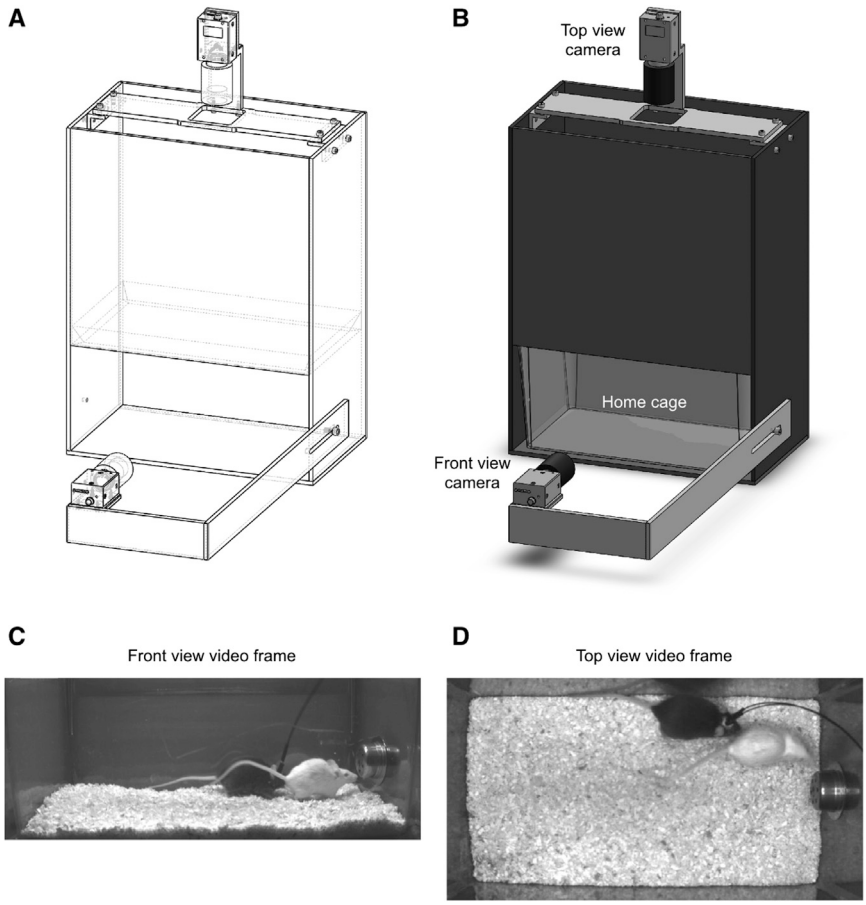

Figure S3. Behavior Equipment Setup Used in This Study, Related to Figure 1

(A and B) Schematic illustrating the customized behavior chamber for the resident-intruder assay. Two synchronized infrared video cameras are placed at a ninety-degree angle. One camera (Basler 601f) is fixed on top of the home cage, and the other (Basler 601f or Basler ace2000-50 gmNIR) is fixed in front of the cage.

(C and D) Representative synchronized video frames taken from front view and top view cameras.

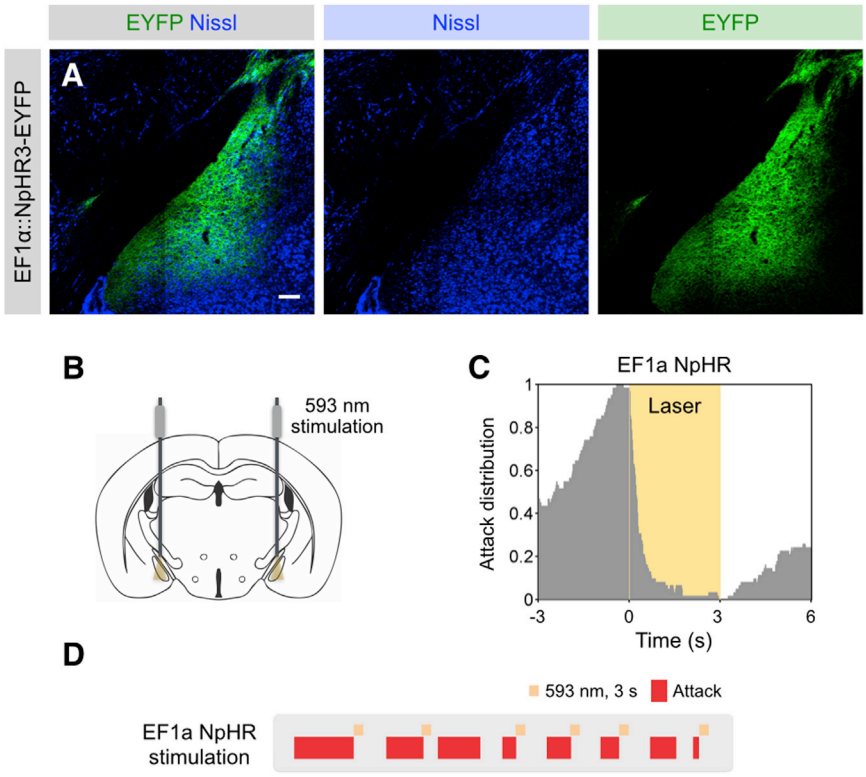

Figure S4. Cre-Independent Optogenetic Silencing of MeApd, Related to Figure 3

(A) Representative images showing the expression of eNpHR3 by the viral vectors AAV2-CMV-Cre and AAV2-EF1α-DIO-eNpHR3-EYFP injected into the MeApd in wild-type C57BL/6N animals. eNpHR3 is tagged with EYFP. Images are taken using multi-area stitching on a confocal microscope; boundary between two adjacent areas can be seen due to uneven illumination. Green, EYFP native fluorescence; blue, fluorescent Nissl stain. Scale bar: 50 μm.

(B) Schematic illustrating optic fiber placement in eNpHR3 virus injected animals.

(C) Distribution of attack episodes (percentage of trials showing attack at different time points) with respect to the initiation of laser illumination in eNpHR3-expressing males tested with male intruders. n = 81 trials.

(D) Representative raster plots illustrating attack episodes in eNpHR3-expressing males tested with intact male intruders in the resident-intruder assay.

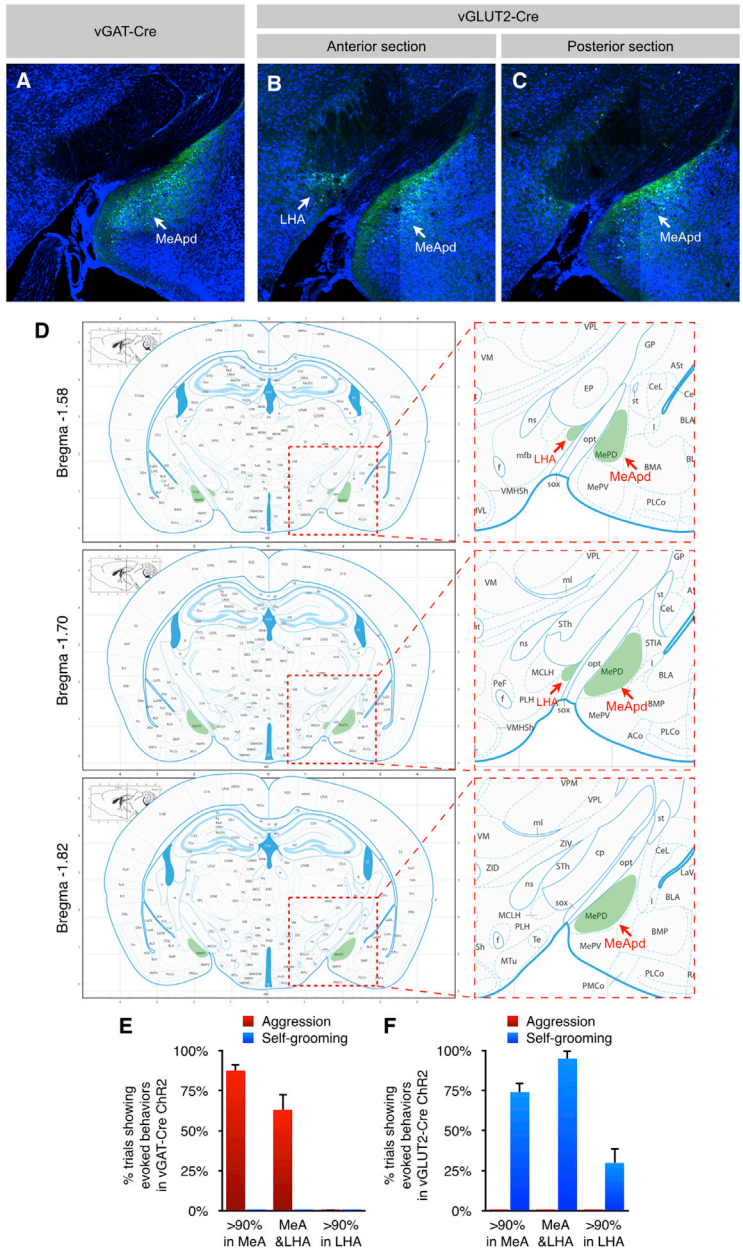

Figure S5. Virus Expression and Optogenetic Activation of MeA and Adjacent LHA in vGAT-Cre and vGLUT2-Cre Animals, Related to Figures 2 and 5

(A–C) Representative images showing the distribution of vGAT$^+$ and vGLUT2$^+$ neurons that trigger attack and self-grooming behavior. The vGAT$^+$ neurons that trigger attack (and other social behaviors) are located within the MeApd (A). vGLUT2$^+$ neurons that trigger self-grooming behavior are enriched in the medial part of the MeApd (B), and are extended to the lateral part of the lateral hypothalamus, a small area near and medial to MeApd (C). Images are taken using multi-area stitching on a confocal microscope; boundary between two adjacent areas can be seen due to uneven illumination. Green, hrGFP native fluorescence; blue, fluorescent Nissl stain.

(D) Schematic showing two anatomical locations the ChR2 virus may potentially be expressed, one in MeApd and another in the lateral part of LHA, at different coronal sections from anterior (upper) to posterior (lower).

(E) Percentage of trials showing evoked attack or self-grooming in vGAT-Cre animals with different virus distribution. This indicates that attack is triggered when the majority of ChR2-expressing neurons are located within MeApd in vGAT-Cre animals.

(F) Percentage of trials showing evoked attack or self-grooming in vGLUT2-Cre animals with different virus distribution. This indicates that self-grooming behavior can also be triggered when the majority of ChR2-expressing neurons are located within MeApd in vGLUT2-Cre animals. A small area of lateral LHA can also elicit self-grooming behavior. This part of LHA has not been previously associated with self-grooming behavior.

Data are mean ± SEM. For vGAT-Cre animals, n = 10 (>90% in MeApd), n = 5 (MeApd & LHA), n = 3 (>90% in LHA). For vGLUT2-Cre animals, n = 8 (>90% in MeApd), n = 8 (MeApd & LHA), n = 5 (>90% in LHA).

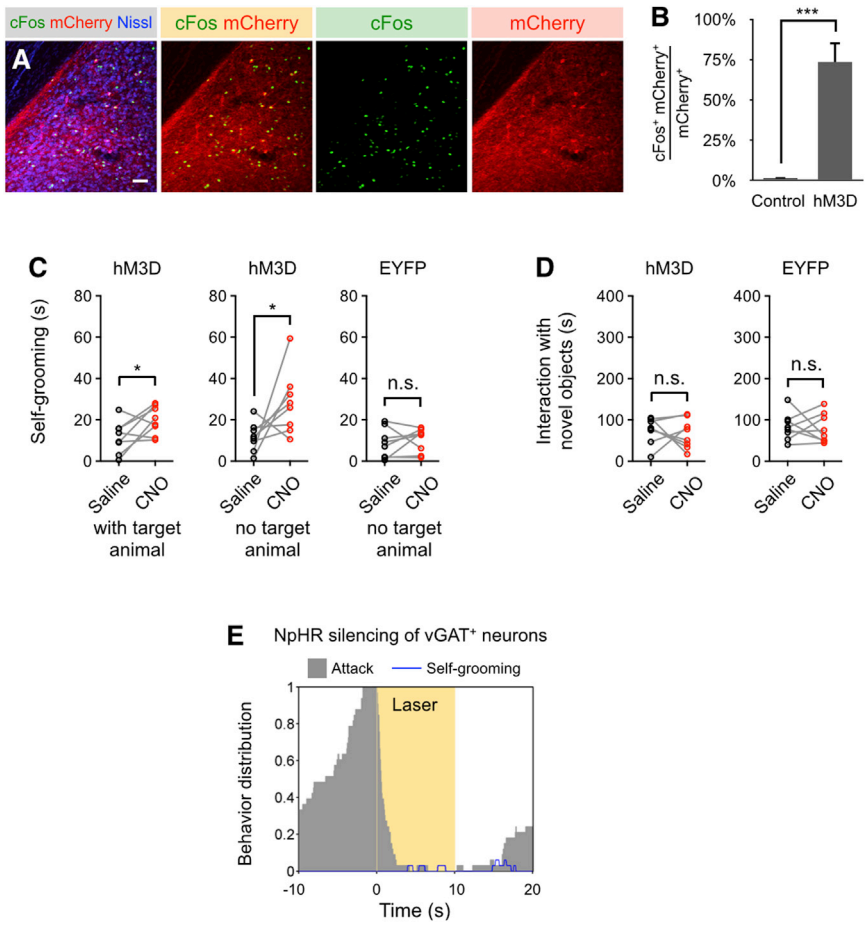

Figure S6. Pharmacogenetic Activation of vGLUT2$^+$ Neurons Reduces Social Interactions, Related to Figure 6

(A and B) c-*fos* induction in hM3D-expressing vGAT$^+$ neurons in solitary animals at 2 hr after CNO administration. Green, c-*fos* immunostaining; red, mCherry native fluorescence; blue, fluorescent Nissl stain. Scale bar: 50 μm. (L) Percentage of total mCherry$^+$ cells expressing c-*fos*.

(C and D) Duration of self-grooming (A) or interaction with novel objects (B) in control or hM3D-expressing animals following saline or CNO administration. CNO results in a moderate increase of self-grooming, which appears to be weaker than what occurs upon ChR2 stimulation. This suggests that acute activation of vGLUT2$^+$ neurons may have a stronger effect on promoting self-grooming behavior than phasic activation.

(E) Distribution of attack (gray area) and self-grooming (blue line) episodes (percentage of trials showing attack and self-grooming, respectively, at different time points) with respect to the initiation of laser illumination in eNpHR-expressing vGAT$^{Cre/+}$ males tested with male intruders. The distribution of attack is also presented in Figure 3H.

Data are mean ± SEM n.s.: $p > 0.05$, *$p < 0.05$, ***$p < 0.001$ (Unpaired t test (B) and Wilcoxon matched-pairs signed rank test (C-D)). n = 8 animals for both hM3D and EYFP control.

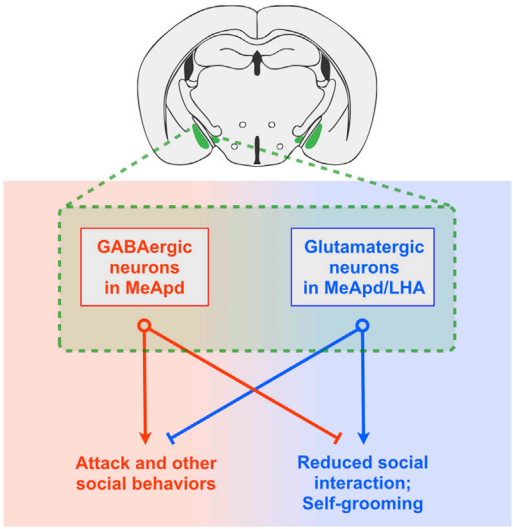

Figure S7. Summary of a Working Model, Related to Figure 7

A schematic showing the opponent control of social and self-grooming behaviors by neighboring, nonoverlapping GABAergic and glutamatergic neurons in MeApd.